Taylor & Francis
Taylor & Francis Group

FMT rescues mice from DSS-induced colitis in a STING-dependent manner

Dan Pu[a]*, Yao Yao[a]*, Chuan Zhou[a]*, Ruixian Liu[a], Zhihong Wang[a], Yan Liu[a], Dandan Wang[a], Binbin Wang[a], Yaohe Wang[b,c], Zhanju Liu[a,d], Zhe Zhang [a], and Baisui Feng [a]

[a]Department of Gastroenterology, The Second Affiliated Hospital of Zhengzhou University, Zhengzhou, China; [b]National Center for International Research in Cell and Gene Therapy, Sino-British Research Centre for Molecular Oncology, Academy of Medical Sciences, Zhengzhou University, Zhengzhou, China; [c]Centre for Biomarkers and Biotherapeutics, Barts Cancer Institute, Queen Mary University of London, London, UK; [d]Department of Gastroenterology, the Shanghai Tenth People's Hospital of Tongji University, Shanghai, China

ABSTRACT

Fecal microbiota transplantation (FMT) is currently a promising therapy for inflammatory bowel disease (IBD). However, clinical studies have shown that there is an obvious individual difference in the efficacy of FMT. Therefore, it is a pressing issue to identify the factors that influence the efficacy of FMT and find ways to screen the most suitable patients for this therapy. In this work, we targeted the stimulator of interferon genes (STING), a DNA-sensing protein that regulates host-defense. By comparing the differential efficacy of FMT in mice with different expression level of STING, it is revealed that FMT therapy provides treatment for DSS-induced colitis in a STING-dependent manner. Mechanistically, FMT exerts a regulatory effect on the differentiation of intestinal Th17 cells and macrophages, splenic Th1 and Th2 cells, as well as Th1 cells of the mesenteric lymph nodes via STING, down-regulating the colonic M1/M2 and splenic Th1/Th2 cell ratios, thereby improving the imbalanced immune homeostasis in the inflamed intestine. Meanwhile, based on the 16SrDNA sequencing of mice fecal samples, STING was found to facilitate the donor strain colonization in recipients' gut, mainly *Lactobacillales*, thereby reshaping the gut microbiota disturbed by colitis. Consequently, we proposed that STING, as a key target of FMT therapy, is potentially a biomarker for screening the most suitable individuals for FMT to optimize treatment regimens and enhance clinical benefit.

Introduction

Inflammatory bowel disease (IBD), including Crohn's disease (CD) and ulcerative colitis (UC), is a chronic immune-mediated inflammatory disorder of the gastrointestinal tract, which is closely related to the dysbiosis of intestinal microbiota.[1,2] One of the promising treatments for IBD is fecal microbiota transplantation (FMT), whereby microbes from healthy donors are transplanted into the intestines of diseased recipients to reshape the disturbed microbiota. However, clinical studies have identified that not every patient with IBD benefits from FMT treatment[3,4] and that patients present varying compatibility with the transplanted strains from the same donor,[5] for reasons and mechanisms that have not been elucidated.

Stimulator of interferon genes (STING), also known as transmembrane protein 173 (TMEM173), regulatory activator of interferon regulatory factor 3

(MITA) and endoplasmic reticulum interferon-stimulating protein (ERIS), is a cytoplasmic DNA sensor that regulates the body's immune defense by recognizing the cytoplasmic DNA from foreign or the host itself.[6,7] Resting STING is localized in the endoplasmic reticulum and is widely expressed in all types of immune and nonimmune cells.[8] Once activated, STING transforms from a dimeric to a multimeric state and moves out of the endoplasmic reticulum to the Golgi apparatus, where it recruits Tank-binding kinase 1 (TBK1) and induces phosphorylation of TBK1. Phosphorylated TBK1 further activates its target proteins, interferon regulatory factor 3 (IRF3) and nuclear factor-kappa B (NF-κB), which enter the nucleus and bind to specific sites in the promoter sequences of target genes, promoting the transcription of type I interferons and inflammatory cytokines. These cytokines in turn exerts host defense functions.

Considering the vital position of STING in the immune surveillance and host defense, which are associated with the colonization of exogenous microbes during FMT therapy, it is of necessity to investigate whether STING affects the efficacy of FMT as well.

To begin with, the effect of STING on colitis was reviewed. Interestingly, STING appears to play a bi-directional role in the pathology of IBD. Some of the studies demonstrated that the activation of STING induces and exacerbates colitis. N153s mice, which are characterized by constitutive activation of STING *in vivo*,[9] exhibit spontaneous colitis at the age of 6 weeks, and the severity of colitis increases progressively with age.[10] Utilizing the mouse colitis model induced by DSS (dextran sodium sulfate), Martin et al. revealed that when mice were administered DMXAA, an agonist of STING, there would be a significant increase in the severity of colitis, along with the conversion of M2 macrophages to the pro-inflammatory M1 subtype.[11] Meanwhile, Ahn et al. also clarified that activation of STING promoted the production of inflammatory factors, such as IL-1β, IL-18, thereby inducing colitis.[12] However, the deficiency of STING increases the susceptibility of mice to colitis as well, leading to a worsening of the disease. It is revealed that STING knockout mice have altered intestinal commensal composition toward a more inflammatory profile compared with WT mice.[13] In addition, the role of STING in maintaining the integrity of the intestine has also been demonstrated in a variety of acute colonic injury models including DSS-induced, T cell-induced and *Salmonella typhi*-induced colitis models, as well as irradiation- and immune-mediated colonic injury models.[13,14] Therefore, based on the current research, it seems that STING acts like a double-edged sword in colitis.

Recently, a meta-analysis of cohort studies demonstrated that moderate-severe IBD patients could achieve more significant remission from FMT than mild-moderate patients.[15] Since both activation and knockout of STING exacerbate colitis, it is of great interest to investigate which type of severe colitis would benefit most from FMT treatment in order to elucidate the role of STING in FMT therapy.

Here, we established the DSS-induced colitis on STING knockout (STING$^{-/-}$), wild-type (WT) and STING-activated mice, and treated them with FMT therapy, respectively. By comparing the severity of colitis and the efficacy of FMT in the three types of mice above, the bidirectional role of STING in the progress of colitis was confirmed. Moreover, for the first time, STING was proved to maximize the benefits of FMT therapy by restraining the pro-inflammatory immune environment in colitis mice, and promoting the colonization of beneficial bacteria (mainly *Lactobacillales*) in the gut of FMT recipients.

Result

Differential enrichment of STING in colonic cell subsets

According to data analysis of the Human Protein Atlas (HPA) database (Figure 1(a)), stimulator of interferon genes (STING) is widely expressed in various tissues, including heart muscle, tonsil, spleen, lung and colon, etc. At single-cell resolution, STING presents low cellular specificity, with expression detected in glandular epithelial cells, endocrine cells, muscle cells, blood and immune cells, etc (Figure 1(b)). Considering the essential roles of intestinal immune cells and epithelial cells in the pathogenesis of IBD, we investigated the expression of STING between the above two cell-types in colons of IBD patients and healthy individuals based on the multi-immunofluorescence technique. As illustrated in Figure 1(c), STING showed a more noticeable co-localization with CD45$^+$ immune cells than EpCAM$^+$ intestinal epithelial cells, both in healthy controls and IBD patients. Furthermore, reanalysis of the publicly available single-cell RNA sequencing data on the Single Cell Portal database (https://singlecell.broadinstitute.org.) showed that STING was significantly enriched in immune cells such as monocytes/macrophages, T cells, etc., in the lamina propria of the colon, regardless of suffering from IBD or not (Figure 1(d)). Consistent with human colon tissues, the similar features were observed in both wild-type (WT) and DSS-induced colitis mice, as evidenced by the fact that STING was significantly enriched in Cd14$^+$Lyz2$^+$ mononuclear macrophages rather than in Epcam$^+$ intestinal epithelial cells (Figure 1(e)). Meanwhile, as the proportion of T-lymphocyte subsets (clusters 0, 1, 2, 4)
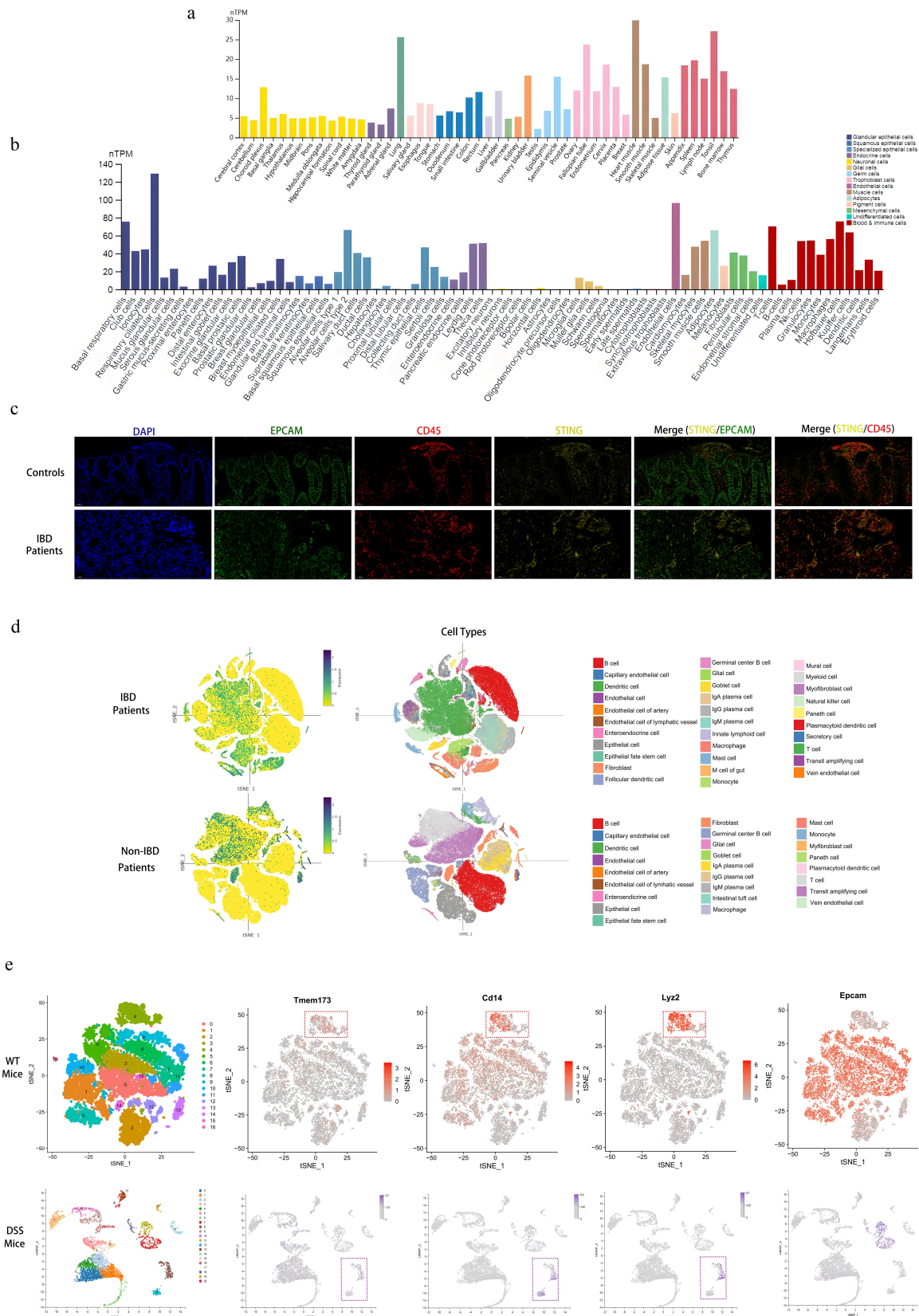
Figure 1. Differential enrichment of STING in colonic cell subsets. (a) Expression of STING in various tissues. (b) Expression of STING in different cells types. (c) Multi-immunofluorescence staining of human colon sections with STING (yellow), CD45 (red), EpCAM (green) antibodies and DAPI (blue). CD45 is an immune cell marker; EpCAM is an epithelial cell marker. Scale bar, 50 μm. (d) Reanalysis of single-cell sequencing data of colon tissues of IBD (upper panel) and non-IBD (bottom panel) patients derived from the single cell

in the inflamed intestine increased, the overall expression of STING in this fraction was correspondingly elevated (Figure 1e, bottom panel). Consequently, STING showed a significant tendency to be differentially enriched in different colonic cellular subsets, implicating the possibility of its complex role in intestinal inflammation.

Acquisition of two mouse models of severe colitis with differential STING activation based on the bidirectional role of STING in DSS-induced colitis in mice

To validate the bidirectional role of STING in colitis, we used three types of mice, namely, STING knockout mice (STING$^{-/-}$), wild-type mice (WT), and STING-activated (DMXAA-treated) mice. At first, the differential activation of STING and its downstream pathway proteins in colons of the above three types of mice were confirmed by assessing the expression levels of phosphorylated STING (pSTING), phosphorylated TBK1 (pTBK1), and phosphorylated IRF3 (pIRF3) (Figure 2(a), left panel). Meanwhile, at the cellular level, DMXAA-treated colon cancer cell line (CT26) and macrophage cell line (RAW264.7) both showed significant activation of STING pathway, which further verified the agonistic effect of DMXAA on STING in different colon cells (Figure 2(a)(, right panel). Next, mice with differential activation of STING as mentioned above were given 2% DSS orally for 10 days to induce colitis (Figure 2(b)). Preliminarily, it was found that WT mice, especially DMXAA-treated mice, showed significantly elevated expression of STING (Figure 2(c)) and phosphorylated STING (phospho-STING) (Figure 2(d)) in the colon after being challenged with DSS, suggesting that STING was activated in DSS-induced colitis. Next, the severity of colitis in each group was compared. It was shown that mice in the STING$^{-/-}$ group experienced significantly lower survival and body weight compared with the WT group, despite the same

baseline levels (Supplementary Figure 1), while the DAI scores were elevated, indicating more severe colitis (Figure 2(e)), in line with the study by Yang et al.[16] Interestingly, the severity of colitis was also remarkably higher in the STING-activated mice in comparison with the WT group, as evidenced by decreased survival and body weight, as well as the enhanced DAI scores (Figure 2(f)), which is consistent with the study by Martin et al.[11] Notably, since the administration of DMXAA from day 0 induced severe colonic inflammation and death in mice,[17] as observed in our pre-experiments, it was decided to start DMXAA treatment from day 5 so as to equalize the severity of colitis in both STING-knockout and STING-activated groups at day 12. The results showed that although both STING$^{-/-}$ and DMXAA-treated mice exhibited shorter colon length (Figure 2 (g),(h)), higher HI scores (Figure 2(i),(j)), higher DAI scores (Figure 2(k)) and worse weight loss (**Figure 2i**) than the WT group on day 12 of the DSS challenge, respectively, no statistical difference in the above metrics were identified between the STING$^{-/-}$ and DMXAA-treated groups, as well as the survival (Figure 2(m)). Therefore, two mouse models of severe colitis were obtained, with differential STING expression and activation but similar disease severity, based on the above treatments.

Considering the bidirectional role of STING in DSS-induced colitis in mice, we further explored the potential mechanisms. Firstly, the intestinal tissue structure of STING$^{-/-}$ mice was investigated. The hematoxylin and eosin (H&E) stain showed that the colonic crypts of STING$^{-/-}$ mice were twisted and distorted, the intestinal submucosal tissues were sparse and edematous, and the number of goblet cells in each colonic crypt was significantly reduced. In contrast, the colonic crypts of WT mice were densely arranged with regular morphology, and the number of goblet cells in each crypt was significantly higher than that of STING$^{-/-}$ mice (Figure 2(n)). Additionally, it was also showed that the depth of colonic crypt (Figure 2(o)) and the expression of the

portal database. (e) Comparison of differential expression of STING between monocytes/macrophages (Cd14$^+$Lyz2$^+$) and intestinal epithelial cells (Epcam$^+$) in the colons of WT mice (upper panel) and DSS-induced colitis mice (bottom panel) based on the GEO database (GSE211578; upper panel) as well as data from single-cell sequencing assays (bottom panel), respectively. The red dashed box (upper panel) and the purple dashed box (bottom panel) mark the STING-enriched subset of Cd14$^+$Lyz2$^+$ cells.
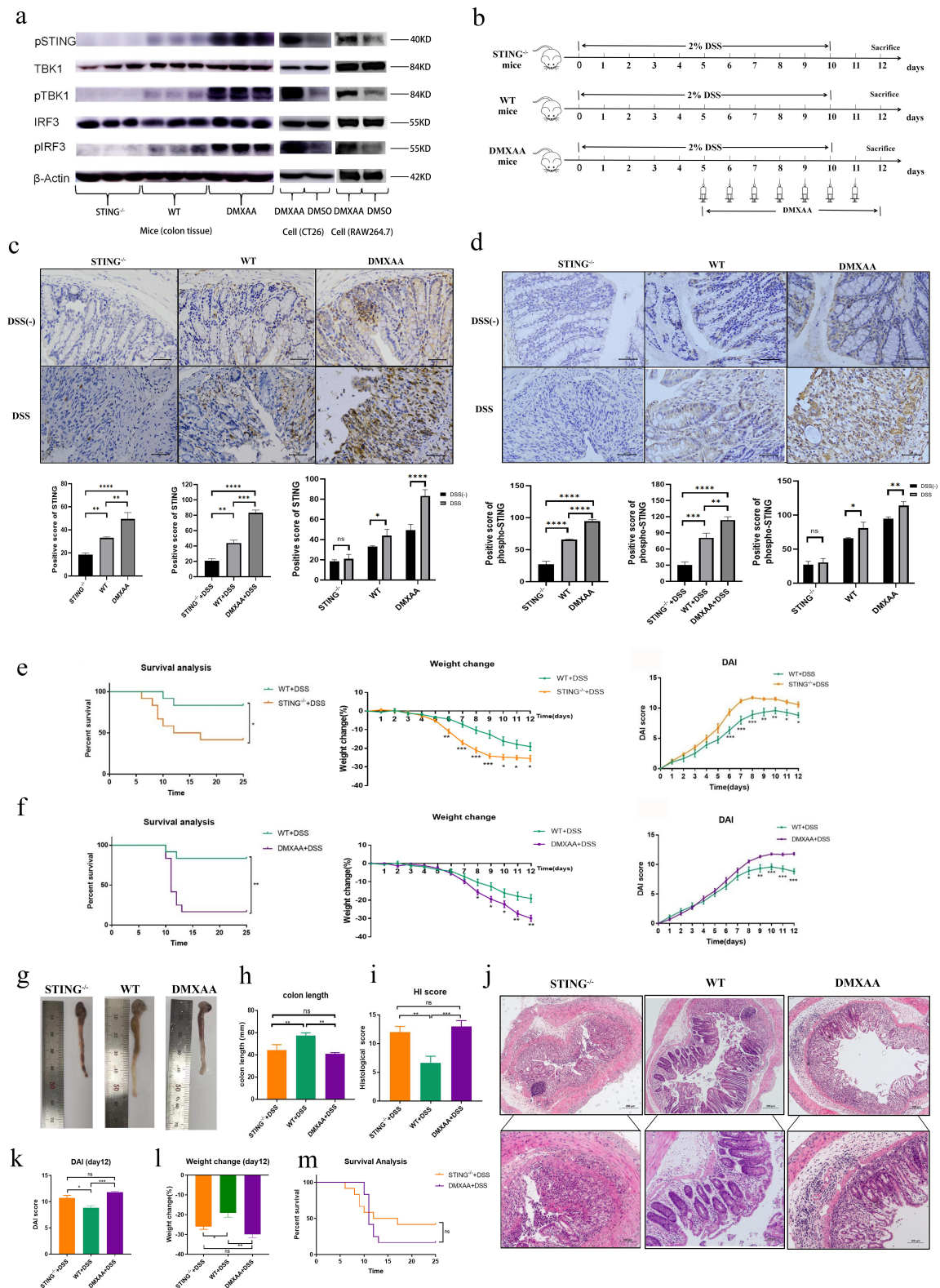
Figure 2. STING plays a bidirectional role in DSS-induced colitis. a) Western Blot band representing the expression of STING-TBK1-IRF3 pathway proteins in the colons of STING$^{-/-}$, WT and STING-activated (DMXAA-treated) mice (left panel), and in the mouse colon cancer cell line CT26 (middle panel) as well as the mouse macrophage cell line RAW264.7 (right panel). b) Experimental treatment protocols. c) Differential expression of STING in the intestine of STING$^{-/-}$, WT and DMXAA-treated mice with or without DSS-induced colitis. d) Differential expression of phospho-STING in the intestine of STING$^{-/-}$, WT and DMXAA-treated mice with or without DSS-induced colitis. e) Survival, weight change and DAI scores of STING$^{-/-}$ mice compared with WT group. f) Survival, weight change and DAI scores of STING-activated (DMXAA-treated) mice compared with WT group. g-h) Comparison of the appearance and length of the colons in

tight junction protein Occludin (Figure 2(p),(q)) were remarkably lower in STING$^{-/-}$ mice than in the WT group. As a consequence, the poor integrity of the intestinal mucosal barrier in STING$^{-/-}$ mice may contribute largely to their greater susceptibility to DSS challenge.

Another question was that why did DMXAA treatment also lead to the exacerbation of DSS-induced colitis in mice? One possible explanation is the effect of DMXAA on the pro-inflammatory properties of macrophages. We examined the production of pro-inflammatory cytokines TNF-α (Figure 2r) and IL-6 (Figure 2(s)) by DMXAA pretreated macrophages upon stimulation with LPS. It was proved that the macrophages cell line (RAW264.7 cells) pretreated with DMXAA were more responsive to LPS and produced more pro-inflammatory cytokines, such as TNF-α and IL-6, than cells not pretreated with DMXAA. RNA-seq further demonstrated that the mRNA expression profiles of macrophages in both NC and DMXAA groups were significantly changed after LPS administration (Supplementary Figure 2a). Csf2, also known as granulocyte-macrophage colony-stimulating factor (GM-CSF), was significantly enriched in LPS-treated macrophages than in the two unstimulated groups (Supplementary Figure 2b). Moreover, in both groups of LPS-treated macrophages, GM-CSF was expressed higher in the STING-activated group (DMXAA group) (Supplementary Figure 2b, 2c). KEGG (Kyoto Encyclopedia of Genes and Genomes) analysis showed that JAK-STAT signaling pathway was significantly enriched in STING-activated macrophages under LPS-induced inflammatory state (Supplementary Figure 2d). Considering that GM-CSF can specifically activate the JAK2-STAT5

signaling pathway to regulate M1 macrophage differentiation,[18–20] we next focused on the activation of the GM-CSF/STAT5 signaling pathway in the above cells. Based on the results of Western Blot, the expression of GM-CSF and phospho-STAT5 proteins was obviously elevated in the STING-activated group compared with the control group (Supplementary Figure 2e). In this regard, it was suggested that DMXAA may promote M1 macrophage differentiation through the GM-CSF /STAT5 signaling pathway and thus worsen colitis. In addition, since TNF-α is the main pro-inflammatory cytokine produced by macrophages in comparison with IL-6 (Figure 2(t)), it is suggested that TNF-α production by STING-activated macrophages is primarily responsible for its pro-inflammatory role in DSS-induced colitis.

STING-activated mice benefit most from the FMT therapy

To determine the correlation between the efficacy of FMT and the activation of STING, we analyzed the differences in altered disease severities of colitis between the FMT-treated and untreated groups among STING$^{-/-}$, WT and STING-activated (DMXAA-treated) mice. Mimicking the clinical treatment pattern, FMT was given from day 5 of DSS administration until day 12 (Figure 3(a)). The STING$^{-/-}$, WT, and DMXAA-treated mice were divided into six groups on the basis of receiving FMT therapy or not (Figure 3(b)). For STING$^{-/-}$ mice (Figure 3 (c)), FMT failed to improve the severity of colitis, as the survival curves (Figure 3(c), left panel), weight change curves (Figure 3(c), middle panel), and DAI curves (Figure 3(c), right

STING$^{-/-}$, WT and STING-activated (DMXAA-treated) groups with DSS-induced colitis. i-j) Representative H&E staining and the comparison of HI scores among STING$^{-/-}$, WT and STING-activated (DMXAA-treated) groups. k) Differences in DAI scores among STING$^{-/-}$, WT and STING-activated (DMXAA-treated) groups at day 12. l) Differences in body weight reduction among STING$^{-/-}$, WT and DMXAA groups at day 12. m) Comparison of the survival rate of STING$^{-/-}$ group and DMXAA-treated group. n) Comparison of intestinal structures between STING$^{-/-}$ and WT mice. o) Comparison of intestinal crypt depth between STING$^{-/-}$ and WT mice. p-q) Differential expression of the colonic tight junction protein Occludin between STING$^{-/-}$ and WT mice. r-s) Differential production of pro-inflammatory cytokines TNF-α and IL-6 by RAW264.7 cells stimulated by LPS in the state with or without DMXAA pretreatment. t) Differential production of TNF-α and IL-6 by DMXAA-treated or untreated RAW264.7cells with or without LPS stimulation. (c, d, h, i, k, l, o-t) Data were shown as mean±SEM. (e, f, m) Data were visualized with Kaplan-Meier curves, differences were tested with log-rank tests; (e, f, o, p, q) Statistical significance was assessed by unpaired Student's t test; (h, i, k, l) Statistical significance was assessed by one-way analysis of variance (one-way ANOVA) with Tukey's multiple comparisons test. (r, s, t) Statistical significance was assessed by two-way ANOVA with Sidak's multiple comparison test. *$p \leq 0.05$, **$p \leq 0.01$, ***$p \leq 0.001$.
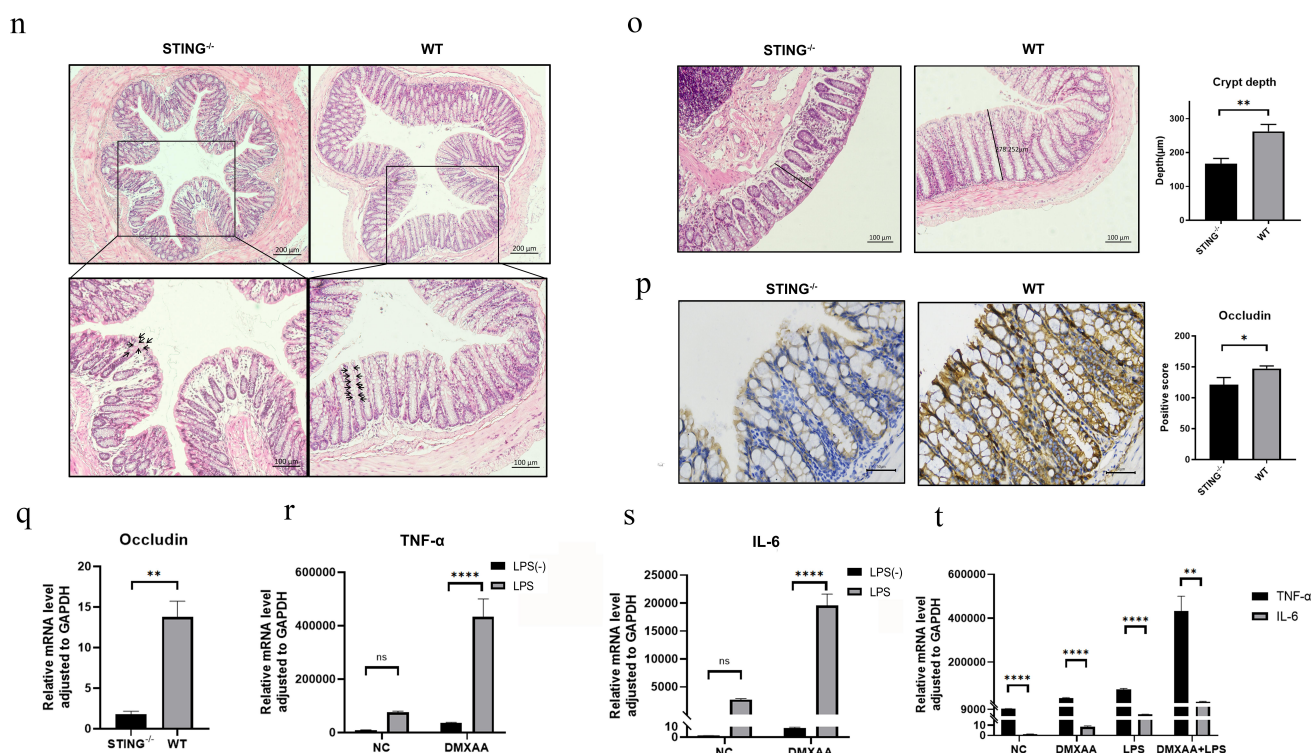
Figure 2. (Continued).

panel) of the FMT-treated and untreated groups almost overlapped. Similarly, for WT mice with colitis, no statistical difference was observed in terms of survival (Figure 3(d), left panel), weight loss (Figure 3(d), middle panel) and DAI scores (Figure 3(d), right panel) between the FMT-treated and untreated groups, even though the above indicators showed a trend of improvement after FMT treatment. However, for the DMXAA-treated groups, FMT significantly alleviated colitis with improved survival (Figure 3(e), left panel), increased body weight (Figure 3(e), middle panel) and downregulated DAI scores (Figure 3(e), right panel). In addition, the severity of colon inflammation of each group was also evaluated at day 12 of the study. Two-way ANOVA revealed that, among the three types of mice with colitis, only the FMT-treated group of DMXAA-treated mice presented statistically significant improvement in HI scores (Figure 3(f),(g)) and colon length (Figure 3(h),(i)), indicating a better efficacy of FMT therapy. Furthermore, although no significant difference was observed in the expression of intestinal TNF-α (Figure 3(j)) and IL-6

(Figure 3(k)) among STING$^{-/-}$, WT, and DMXAA-treated mice in the absence of DSS treatment, colonic tissues of DMXAA-treated mice expressed more TNF-α (Figure 3(l)) after being challenged with DSS, whereas STING$^{-/-}$ mice possessed more IL-6 (Figure 3(m)). Noticeably, unlike the STING$^{-/-}$ and WT mice, the expressions of both TNF-α (Figure 3(n)) and IL-6 (Figure 3(o)) were significantly downregulated in the colon of DMXAA-treated mice after FMT therapy. As a result, among the three types of mice with differential activation of STING, only the DMXAA-treated (STING-activated) mice benefited the most from FMT treatment, suggesting that FMT provides therapeutic treatment for colitis in a STING-dependent manner.

STING enhances the negative regulation effect of FMT on pro-inflammatory immune cell subsets in lamina propria (LP) and mesenteric lymphocyte nodes (MLN)

To further investigate the mechanism by which STING affects the efficacy of FMT, we first evaluated the influence of STING on the intestinal
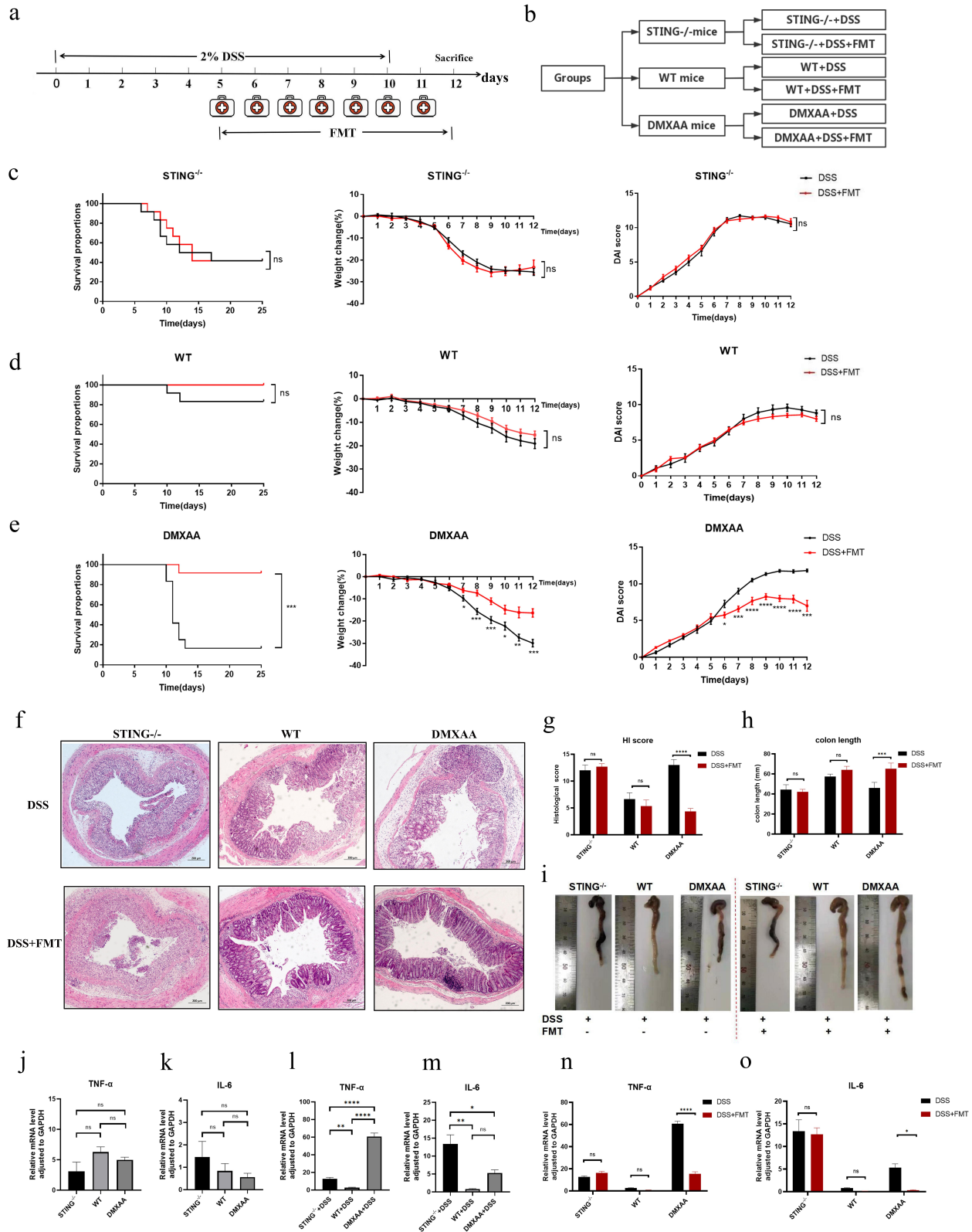
Figure 3. STING facilitates maximum benefit from FMT treatment in mice with colitis. (a) Experimental treatment protocols. (b) Grouping scheme of the experiment. (c) Comparison of survival, weight change, and DAI scores between the FMT-treated and untreated groups of STING$^{-/-}$ mice. (d) Comparison of survival, weight change, and DAI scores between the FMT-treated and untreated groups of WT mice. (e) Comparison of survival, weight change, and DAI scores between the FMT-treated and untreated groups of STING-activated (DMXAA-treated) mice. (f–g) Representative H&E staining and the comparison of HI scores in each group. (h–i) Representative colon pictures and the comparison of colon length in each group. (j–k) Differential TNF-α and IL-6 production in

immune microenvironment during FMT therapy by flow cytometry. As the major subset of CD4^{+} T cells, Th1 cells, which primarily produce interferon (IFN)-γ and tumor necrosis factor (TNF), have been shown to be closely associated with the pathology of IBD.[21,22] In the absence of FMT administration, STING did not significantly affect the percentage of Th1 cells in LP (Figure 4(a),(b)); even in MLN, Th1 cells showed a trend to increase with the expression of STING (Figure 4(c),(d)). However, when treated with FMT, only the STING-activated mice exhibited a significant reduction in Th1 cells in both the LP (Figure 4(a), (e)) and MLN (Figure 4(c),(f)) compared with their untreated counterparts.

Th17 cells, another important cell subset of CD4^{+} T cells, are significantly enriched in the colon of IBD patients and animal models.[23] According to our findings (Figure 4(g)), although Th17 cells showed a tendency to increase along with the expression of STING among the FMT-untreated groups (Figure 4 (h)), the two-way ANOVA indicated that only the STING-activated colitis mice experienced the greatest decrease in the proportion of Th17 cells after FMT treatment (Figure 4(i)).

Apart from the enrichment of T lymphocytes, the increased proportion of intestinal macrophages, which are predominantly pro-inflammatory M1 subtypes, is another important factor in the progression of IBD.[24,25] As the expression of STING increased, percentages of intestinal macrophages (Figure 4(j)) and the M1/M2 ratio (Figure 4(k)) in FMT-untreated groups exhibited a progressive growth, which is consistent with the study of Shmuel-Galiaet al.[10] However, unlike STING^{−/−} and WT mice, STING-activated mice showed significantly downregulated percentages of intestinal macrophages (Figure 4(i)) as well as M1/M2 ratios (Figure 4(m)) after FMT therapy compared with the untreated group.

These data suggested that STING enhanced the efficiency of FMT in downregulating the percentage of pro-inflammatory Th1 cells, Th17 cells, macrophages, and M1/M2 ratio in the intestinal microenvironment, thereby contributing to the elimination of intestinal inflammation.

STING enhances the negative regulatory effect of FMT on pro-inflammatory immune cell subsets in spleen

In addition to alterations in the subsets of intestinal immune cells, changes in the overall immune system of the body suffering from colitis were also of concern. As the largest immune organ, the spleen plays an important role in assessing the total inflammatory status of the body.[26] Therefore, we investigated the alteration of immune cell subsets in the spleen of colitis mice after FMT therapy in the context of differential STING expression as well. It was observed that the percentages of splenic Th1 (Figure 5(a),(b)) and Th2 (Figure 5(c),(d)) cells showed a progressive tendency to raise with increasing STING expression in the absence of FMT administration. However, after FMT treatment, only the STING-activated mice exhibited lower proportions of Th1 (Figure 5(a),(e)) and Th2 cells (Figure 5(c),(f)) in the FMT-treated group than the untreated counterparts. Moreover, the Th1/Th2 ratio, one of the indicators reflecting the dynamic homeostasis of immune system *in vivo*, was significantly upregulated in both the STING^{−/−} and STING-activated mice compared with the WT group (Figure 5(g)), corresponding to the severity of the disease. Interestingly, in spite of the similar level of Th1/Th2 ratio in DSS-challenged STING^{−/−} and STING-activated mice, only the STING-activated mice showed a statistically significant decrease in Th1/Th2 ratios after FMT treatment (Figure 5(h)), indicating a pronounced improvement in the immune disorder. Accordingly, STING enhanced the negative regulation of FMT on the proportions of Th1 and Th2 cells, as well as the Th1/Th2 ratio in the spleen.

---

the colons of STING^{−/−}, WT, and DMXAA-treated mice without DSS-induced colitis. (l-m) Differential TNF-α and IL-6 production in the colons of STING^{−/−}, WT, and DMXAA-treated mice with DSS-induced colitis. (n) Differential reduction of pro-inflammatory cytokines TNF-α and IL-6 in the colon of STING^{−/−}, WT, and DMXAA-treated colitis mice after FMT therapy. Data were shown as mean ± SEM. (c, d, e; left panel) data were visualized with Kaplan-Meier curves, differences were tested with log-rank tests; (c, d, e; middle and right panel) statistical significance was assessed by unpaired Student's t test; (j, k, l, m) Statistical significance was assessed by one-way analysis of variance (one-way ANOVA) with Tukey's multiple comparisons test; (g, h, n, o) statistical significance was assessed by two-way ANOVA with Sidak's multiple comparison test. *$p \leq 0.05$, **$p \leq 0.01$, ***$p \leq 0.001$, ****$p \leq 0.0001$.
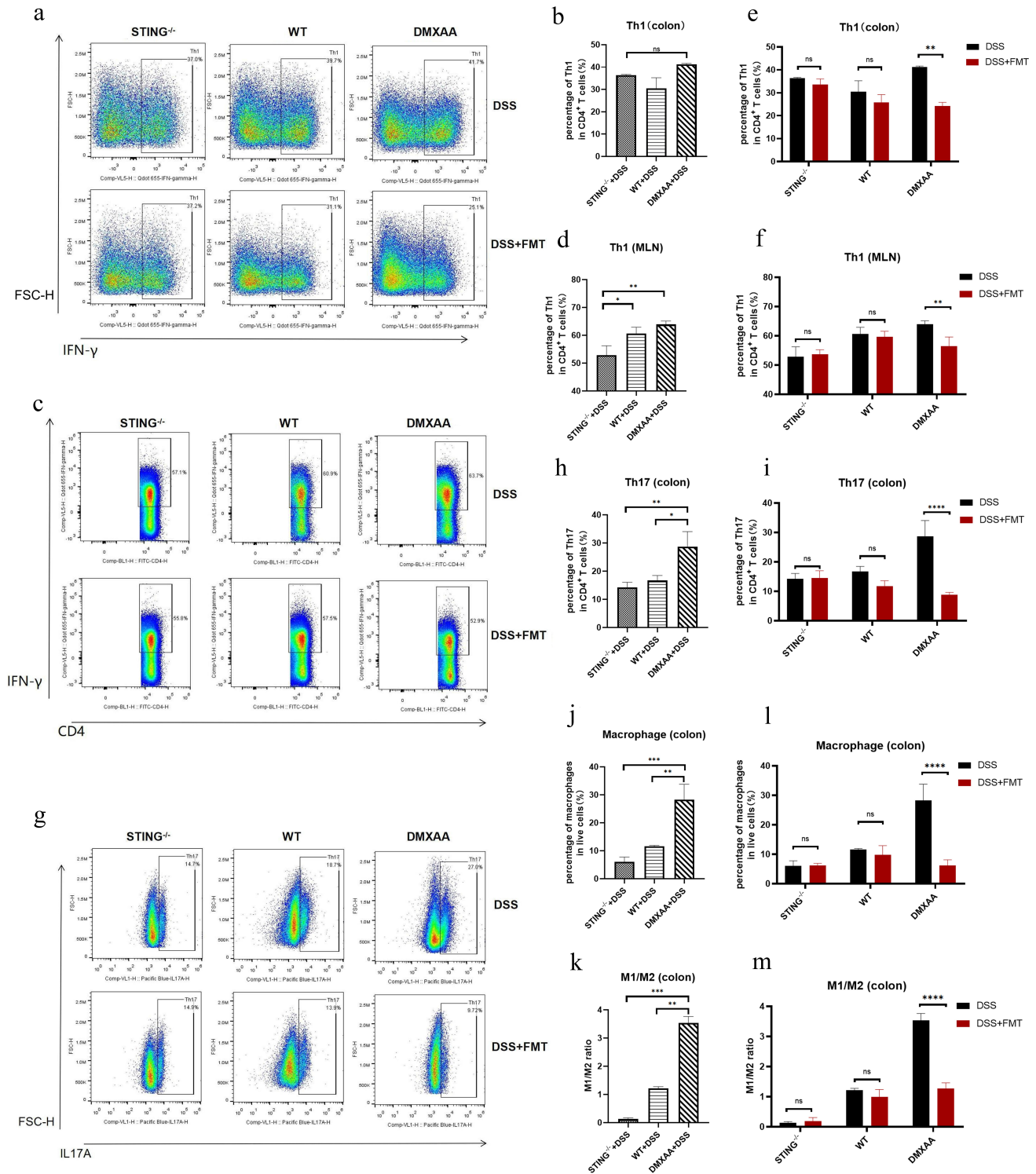
Figure 4. STING enhances the negative regulation effect of FMT on pro-inflammatory immune cell subsets in LP and MLN. (a) Representative flow cytometry plots of Th1 cells in the colon of each group. (b) Comparison of the proportions of intestinal Th1 cells among the FMT-untreated groups. (c) Representative flow cytometry plots of Th1 cells in the MLN of each group. (d) Comparison of the proportions of Th1 cells in MLN among the FMT-untreated groups. (e) differences in the percentage changes of intestinal Th1 cells between the FMT-treated and FMT-untreated groups among STING$^{-/-}$, WT and STING-activated (DMXAA-treated) mice. (f) Differences in the percentage changes of Th1 cells in MLN between the FMT-treated and FMT-untreated groups among STING$^{-/-}$, WT and STING-activated (DMXAA-treated) mice. (g) Representative flow cytometry plots of Th17 cells in the colon of each group. (h) Comparison of the proportions of intestinal Th17 cells in the FMT-untreated groups. (i) Differences in the percentage changes of intestinal Th17 cells between the FMT-treated and FMT-untreated groups among STING$^{-/-}$, WT and STING-activated (DMXAA-treated) mice. (j) Comparison of the proportions of intestinal macrophages among the FMT-untreated groups. (k) Comparison of the intestinal M1/M2 ratio among
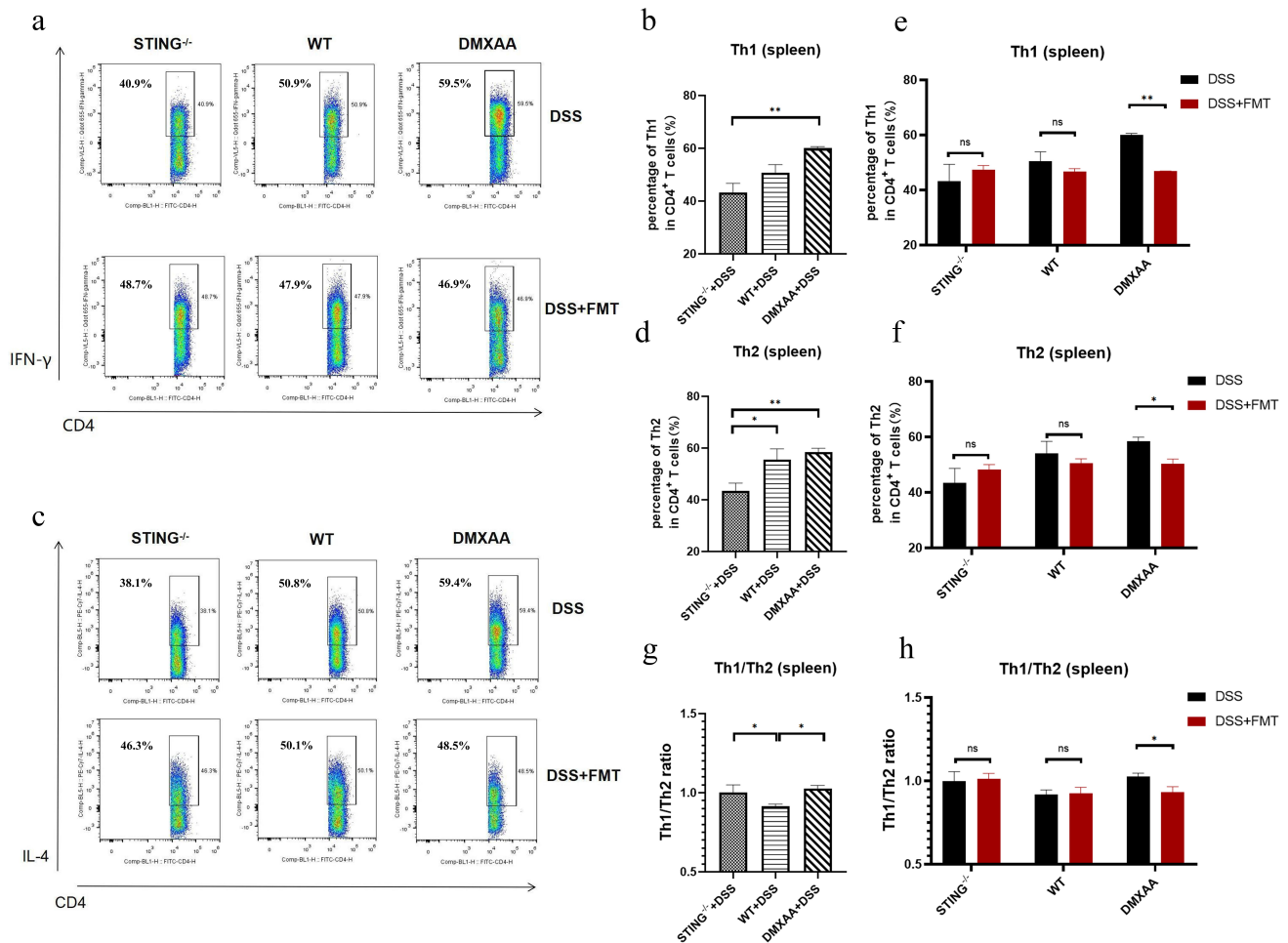
Figure 5. STING enhanced the negative regulatory effect of FMT on pro-inflammatory immune cell subsets in spleen. (a) Representative flow cytometry plots of Th1 cells in the spleen of each group. (b) Comparison of the proportions of splenic Th1 cells among the FMT-untreated groups. (c) Representative flow cytometry plots of Th2 cells in the spleen of each group. (d) Comparison of the proportions of splenic Th2 cells among the FMT-untreated groups. (e) Differences in the percentage changes of splenic Th1 cells between the FMT-treated and untreated groups among STING$^{-/-}$, WT and STING-activated (DMXAA-treated) mice. (f) Differences in the percentage changes of splenic Th2 cells between the FMT-treated and untreated groups among STING$^{-/-}$, WT and STING-activated (DMXAA-treated) mice. (g) comparison of the splenic Th1/Th2 ratios among the FMT-untreated groups. (h) Differences in the alterations of splenic Th1/Th2 ratios between the FMT-treated and untreated groups among STING$^{-/-}$, WT and STING-activated (DMXAA-treated) mice. Each group consists of 3 biological replicates; data were shown as mean ± SEM. (b, d, g) Statistical significance was assessed by one-way ANOVA with Tukey's multiple comparisons test; (e, f, h) statistical significance was assessed by two-way ANOVA with Sidak's multiple comparison test. *$p \leq 0.05$, **$p \leq 0.01$.

STING increases the similarity of intestinal microbiota between diseased recipients and healthy donors after FMT treatment

It is widely accepted that successful colonization of transplanted bacteria is essential for the immunotherapeutic role of FMT since they intervene in the intestinal inflammatory process through crosstalk with various immune cells.[27] Given that the activation of STING significantly enhanced the negative regulation of FMT on pro-

the FMT-untreated groups. (i) Differences in the percentage changes of intestinal macrophage between the FMT-treated and FMT-untreated groups among STING$^{-/-}$, WT and STING-activated (DMXAA-treated) mice. (m) Differences in the alterations of intestinal M1/M2 ratios between the FMT-treated and FMT-untreated groups among STING$^{-/-}$, WT and STING-activated (DMXAA-treated) mice. Each group consists of 3 biological replicates; data were shown as mean ± SEM. (b,d,h,j,k) Statistical significance was assessed by one-way ANOVA with Tukey's multiple comparisons test; (e,f,i,l,m) statistical significance was assessed by two-way ANOVA with Sidak's multiple comparison test. *$p \leq 0.05$, **$p \leq 0.01$, ***$p \leq 0.001$, ****$p \leq 0.0001$.
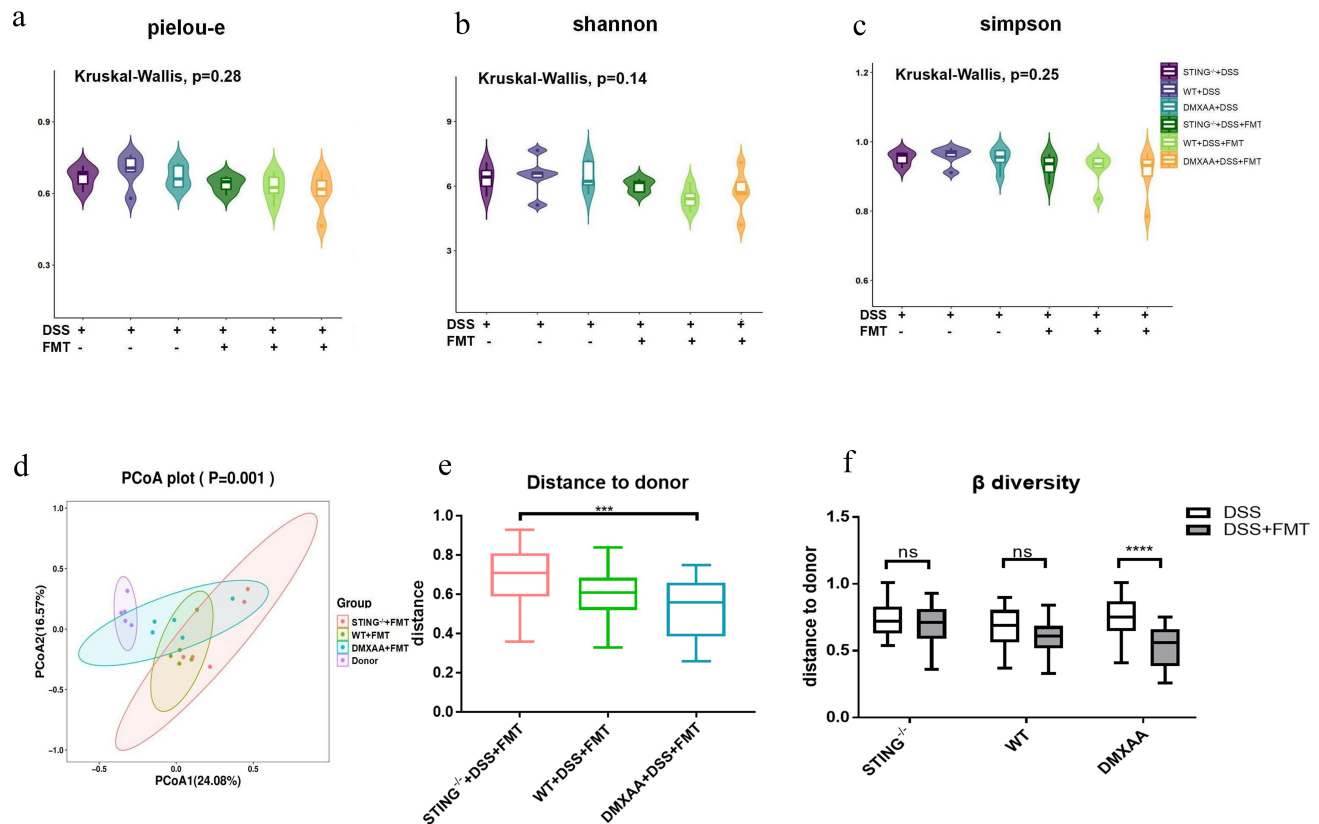
Figure 6. STING affects the similarity of gut microbiota between diseased recipients and healthy donors after FMT treatment. (a-c) α-diversity of the intestinal microbiota in each group, measured by pielou-e, Shannon and Simpson indices, respectively. (d) PCoA plot of intestinal microbiota in FMT-treated groups of STING$^{-/-}$, WT, STING-activated (DMXAA-treated) colitis mice and the healthy donors based on Bray-Curtis algorithm. (e) Comparison of the differences in the distance between the gut microbiota of the three FMT treatment groups and the healthy donors, respectively. (f) Differences in the alterations of β-diversity (measured by the distance to donor) between the FMT-treated and untreated groups among STING$^{-/-}$, WT and STING-activated (DMXAA-treated) mice. Each group consists of 5 biological replicates; data were shown as mean ± SEM. (a, b, c) statistical significance was assessed by Kruskal-Wallis test; (e) statistical significance was assessed by one-way ANOVA with Tukey's multiple comparisons test; (f) statistical significance was assessed by two-way ANOVA with Sidak's multiple comparison test. ***$p \leq 0.001$, ****$p \leq 0.0001$.

inflammatory immune cells, it is hypothesized that STING may influence the colonization efficacy of healthy gut microbes during FMT, thereby affecting its therapeutic outcomes. To characterize the effect of STING on the colonization of the recipients' intestine by transplanted bacteria during FMT therapy, feces were collected for 16S rDNA sequencing from each groups of colitis mice and healthy donors. It was found that STING did not affect the α-diversity of the intestinal bacteria of mice with colitis, whether administered with DSS only or in combination with FMT therapy. Here, α-diversity was evaluated based on a combination of the pielou-e score (Figure 6(a)), Shannon score (Figure 6(b)) and Simpson score (Figure 6(c)), which

represent group evenness, richness, or both, respectively. However, for the FMT-treated groups, β-diversity, an index representing the similarity of microbial communities between different groups measured by the distance to donor, was found to decrease progressively with the increasing STING expression (Figure 6(d),(e)), a feature not been observed among the three FMT-untreated groups. The most pronounced alteration in β-diversity between the FMT-treated and untreated groups was observed in STING-activated mice, followed by WT mice, whereas β-diversity in STING$^{-/-}$ mice remained almost unchanged in both the FMT-treated and untreated group with the same median level (Figure 6(f)). Two-way ANOVA demonstrated

that compared with STING$^{-/-}$ and WT mice, only the STING-activated mice presented statistically significant differences in β-diversity between the FMT-treated and untreated group, suggesting that STING enhances the similarity between the intestinal microbiota of the recipients and the healthy donors after FMT therapy.

STING promotes the colonization of probiotic lactobacillales and its subordinate bacteria in the recipients' gut

Next, we evaluated the distribution of each taxon derived from healthy donors in the FMT-treated groups with different STING expression. Initially, linear discriminant analysis effect size (LEfSe) analysis was performed on the intestinal microbiota of the three FMT-treated groups to identify biomarkers associated with STING (Figure 7(a)). Notably, although the FMT-treated groups of STING$^{-/-}$, WT and STING-activated mice were included simultaneously, the LEfSe analysis ultimately screened out only the characteristic intestinal bacteria of the STING$^{-/-}$ and DMXAA groups, suggesting that the composition of the intestinal bacteria of WT mice after FMT treatment was intermediate between the STING$^{-/-}$ and DMXAA groups, which is consistent with the results of the β-diversity analysis. According to the LEfSe analysis, 12 taxa including *Lactobacillales* and its subordinate taxa *Lactobacillaceae*, *Ligilactobacillus*, *Ligilactobacillus-unclassified spp*. and *HT002* were significantly enriched in the FMT-treated group of STING-activated mice, while 9 taxa including *Allobaculum* and *Allobaculum-unclassified spp*. were significantly enriched in the FMT-treated group of STING-/- mice (Figure 7(b)).

Furthermore, the aforementioned bacteria was also revalidated at the order, family, genus level, respectively, for their differential distribution in each group. At the Order (Figure 7(c)) and Family levels (Figure 7(d)), no significant differences in the abundance of *Lactobacillales* and *Lactobacillaceae* was observed among FMT-untreated STING$^{-/-}$, WT, and STING-activated mice (Supplementary Figure 3). However, after FMT treatment, the abundance of these bacteria gradually increased with the enhancement of STING expression (Figure 7(e),(f)), which was consistent with the features of the microbiota composition among the three types of mice without DSS challenge (Supplementary Figure 4a-d). Similarly, at the Genus level (Figure 7(g)), the abundance of *Ligilactobacillus* (Figure 7(h)) and *HT002* (Figure 7(i)) in the FMT-treated group gradually increased with higher STING expression, in line with the characterization of the three types of mice which were not challenged with DSS (Supplementary Figure 4e-g). In contrast, the abundance of *Allobaculum* (Figure 7(j)) declined progressively along with the STING activation among FMT-treated groups. Two-way ANOVA demonstrated more clearly that among the three types of mice with differential expression of STING, only the activation group experienced the most significant enrichment of *Lactobacillales*, *Lactobacillaceae*, as well as their subordinate *Ligilactobacillus* and *HT002* after FMT treatment compared with the untreated ones (Figure 7(k)). As a consequence, it is concluded that STING contributes to the colonization of *Lactobacillales* and its subordinate bacteria in the intestine of mice with colitis.

To further investigate the potential mechanism by which DMXAA promotes the colonization of *Lactobacillales*, a co-culture experiment was designed (Supplementary Figure 5). As mentioned previously, STING, although predominantly enriched in intestinal macrophages, is still expressed to a small extent in epithelial cells. Therefore, transwell chambers were used to clarify exactly which cell-type with DMXAA affects *Lactobacillales* colonization. Intestinal epithelial cells CT26 were categorized into two groups: co-cultured and mono-cultured. Further detailed groupings were performed based on whether the macrophages RAW264.7 co-cultured with CT26 received DMXAA and/or LPS stimulation (Supplementary Figure 6a). Co-cultured or mono-cultured CT26 cells were co-incubated with *L. murinus*, a species of *Lactobacillales*, for 3 h and then subjected to the FISH assay to visualize and quantify the amount of adherent bacteria. The results showed that CT26 cells co-cultured with RAW264.7 receiving DMXAA pretreatment exhibited significant *Lactobacillales* adhesion efficacy irrespective of whether LPS stimulation was given or not, which was not observed in the four mono-
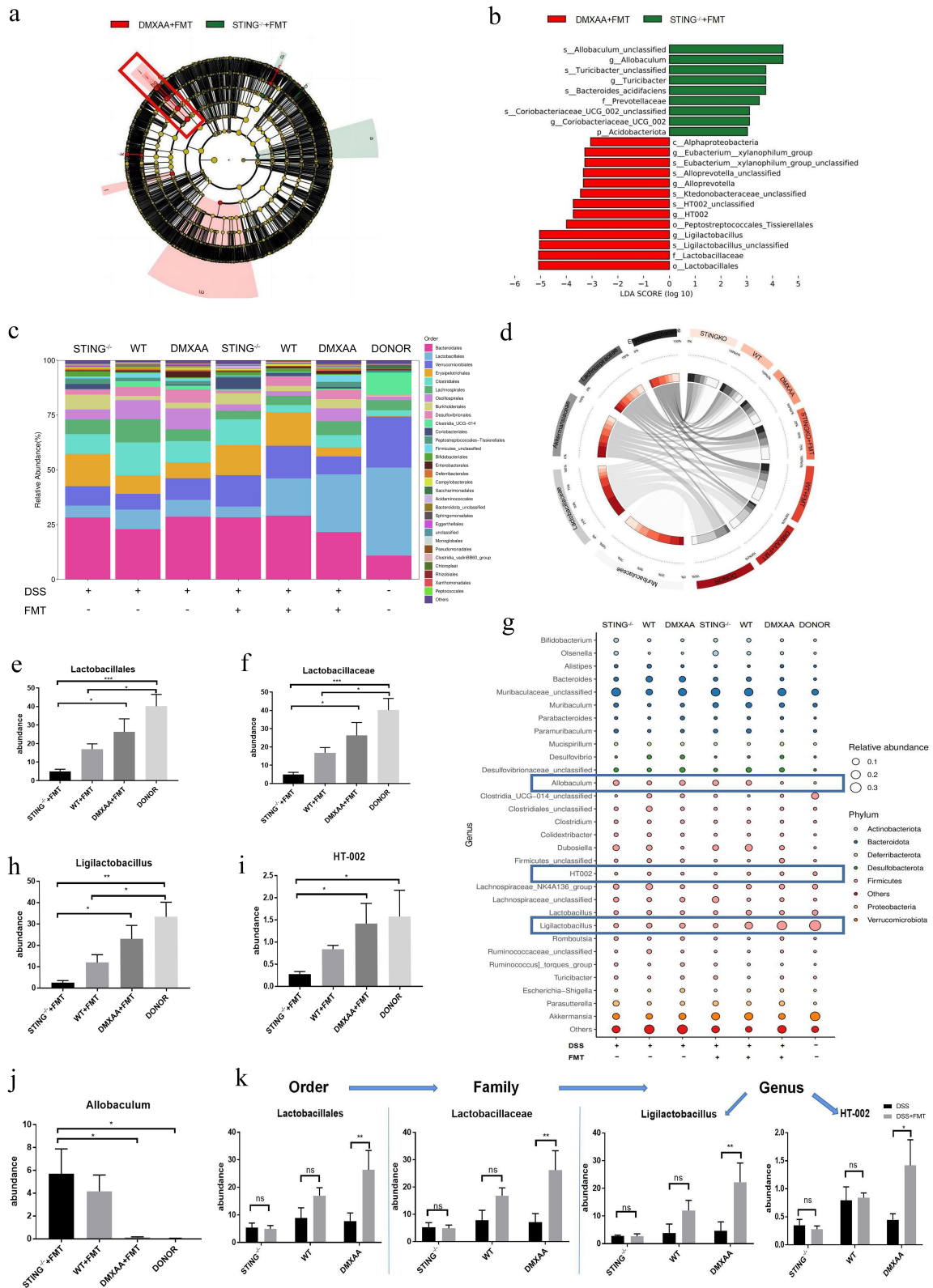
Figure 7. STING promotes the colonization of probiotic *Lactobacillales* and its subordinate bacteria in the recipients' gut. a-b) Cladogram (a) and LDA bar plot (b) based on the LEfSe algorithm showing the significantly enriched intestinal microbiota in the FMT-treated groups with differential expression of STING, respectively. (c) the abundance of TOP30 intestinal microbiota in the experimental groups and the donors at the order level. (d) the abundance of TOP30 intestinal microbiota in the experimental groups and the donors at the family level. (e) Differences in the abundance of *Lactobacillales* in the intestine of FMT-treated groups and the healthy donors. (f) Differences in the abundance of *Lactobacillaceae* in the intestine of FMT-treated groups and the healthy donors. (g) the abundance of TOP30 intestinal microbiota in the experimental groups and the donors at the genus level. (h-j) Differences in the

cultured groups (Supplementary Figure 6b). This implied that STING-activated macrophages promote the adhesion of epithelial cells to *Lactobacillales*. RNA-seq-based GO (Gene Ontology) and KEGG analyses further revealed that the biological process of symbiont-host adhesion was significantly enriched in CT26 cells cocultured with STING-activated RAW264.7 cells (Supplementary Figure 6c), and signaling pathways associated with cell adhesion were also markedly upregulated (Supplementary Figure 6d). More interestingly, the CD14 molecule, which serves as a high-affinity pattern recognition receptor for *Lactobacillales*' adhesin Lipoteichoic acid (LTA), was significantly overexpressed in epithelial cells co-cultured with STING-activated macrophages (Supplementary Figure 6e, 6f). This indicated that STING-activated macrophages may enhance the adhesion of intestinal epithelial cells to *Lactobacillales* by up-regulating CD14 expression in epithelial cells.

STING facilitates the remodeling effect of FMT therapy on intestinal metabolic disorders in mice with colitis

To determine the alterations in intestinal metabolism affected by STING during FMT therapy, we employed the Phylogenetic Investigation of Communities by Reconstruction of Unobserved States (PICRUSt2) software to analyze the levels of intestinal metabolism in the FMT-treated groups of STING$^{-/-}$, WT and STING-activated mice as well as the healthy donors. The top 12 KEGG categories with the most significant differences ($p < 0.01$) were identified, positively or negatively correlated with the expression of STING (Figure 8 (a)). Four metabolic pathways that play an anti-inflammatory role in colitis, including tetracycline biosynthesis,[28,29] fatty acid biosynthesis[30] and nucleotide metabolism,[31,32] were progressively upregulated with enhanced STING expression. In contrast, eight pro-inflammatory metabolic pathways, including histidine metabolism,[33] proteasome,[34] streptomycin biosynthesis,[35] as well as arginine and proline metabolism,[36] tended to be progressively downregulated with the increase in STING expression. Spearman's correlation analysis revealed that the TOP30 intestinal bacteria could be clustered based on the 12 differential KEGG categories mentioned above (Figure 8(b)). In particular, 10 of the TOP30 taxa, including *Lactobacillales*, *Verrucomicrobiales*, *Clostridia-UCG-014*, were positively associated with the four anti-inflammatory metabolic pathways and negatively associated with the eight pro-inflammatory metabolic pathways. It is worth noting that the aforementioned correlation was strongest for *Lactobacillales*. Consequently, STING assists FMT in restoring the homeostasis of intestinal metabolism, which may be associated with a good colonization of beneficial bacteria such as *Lactobacillales*.

Hyperactivation of the STING pathway in patients with severe IBD may contribute to the benefit from FMT therapy

Considering the potentiating role played by STING during FMT treatment, we wondered which group of IBD patients had enriched STING in their intestines so that they could benefit most from FMT therapy. According to the analysis of the GEO database, the mRNA expression of STING and its downstream genes TBK1 and IRF3 were significantly higher in both UC (Figure 9(a)) and CD patients (Figure 9(b)) than in healthy controls. Furthermore, differential expressions of STING, phosphorylated STING (phospho-STING), TBK1, phosphorylated TBK1 (phospho-TBK1), IRF3, and phosphorylated IRF3 (phospho-IRF3) proteins of the STING-TBK1-IRF3 pathway in colons of UC (Figure 9(c)) or CD (Figure 9(d)) patients were examined at different levels of disease activity, respectively. IHC analysis revealed that the

abundance of *Ligilactobacillus*, *HT-002* and *Allobaculum* in the intestine of FMT-treated groups and the healthy donors. (k) Two-way ANOVA comparing the differences in colonization of the *Lactobacillales*, *Lactobacillaceae*, *Ligilactobacillus* and *HT-002* in the inflamed intestine among STING$^{-/-}$, WT and STING-activated (DMXAA-treated) groups. Each group consists of 5 biological replicates; data were shown as mean ± SEM. (e, f, h, i, j) Statistical significance was assessed by one-way ANOVA with Tukey's multiple comparisons test; (k) statistical significance was assessed by two-way ANOVA with Sidak's multiple comparison test. *$p \leq 0.05$, **$p \leq 0.01$, ***$p \leq 0.001$.
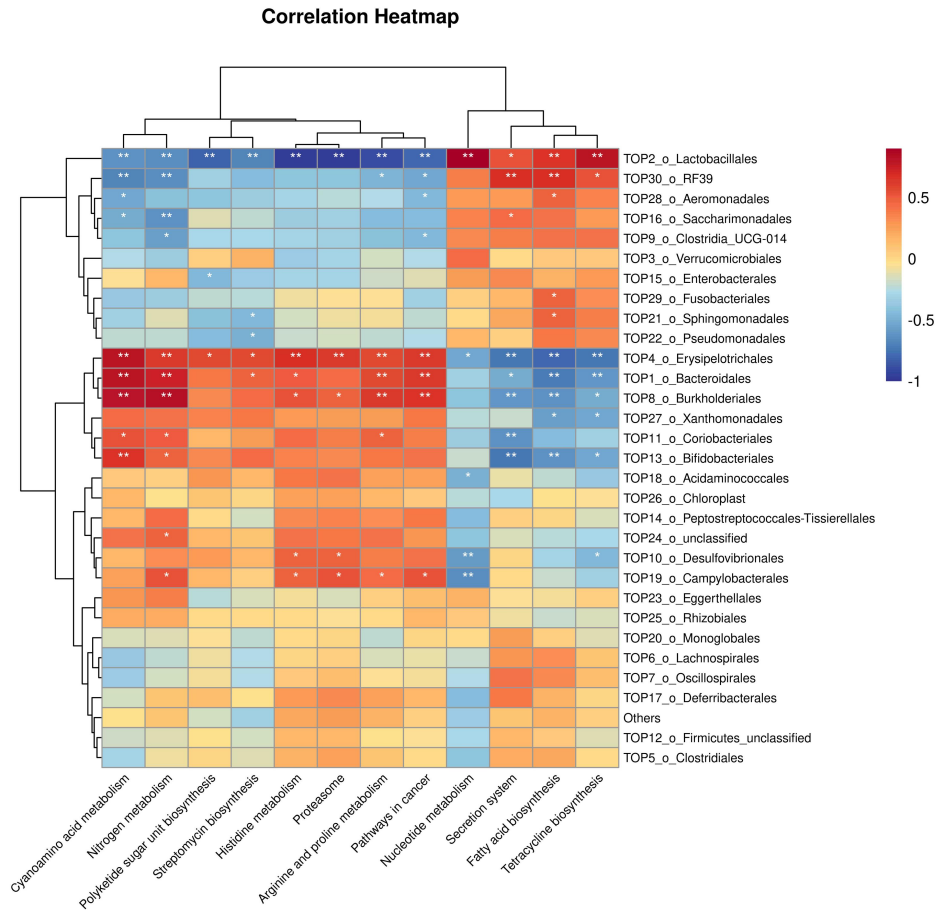
A
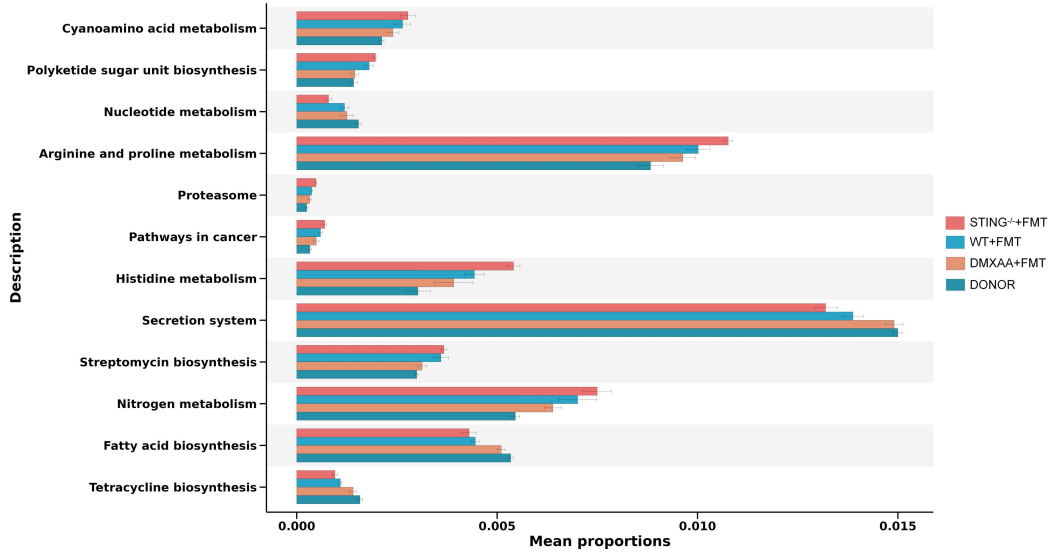
B

Figure 8. STING assists FMT therapy to reshape disturbed intestinal metabolism in mice with colitis. (a) Differential TOP12 KEGG pathways associated with colitis in each FMT-treated groups and the donor group as predicted by PICRUSt2. (b) Correlation heatmap
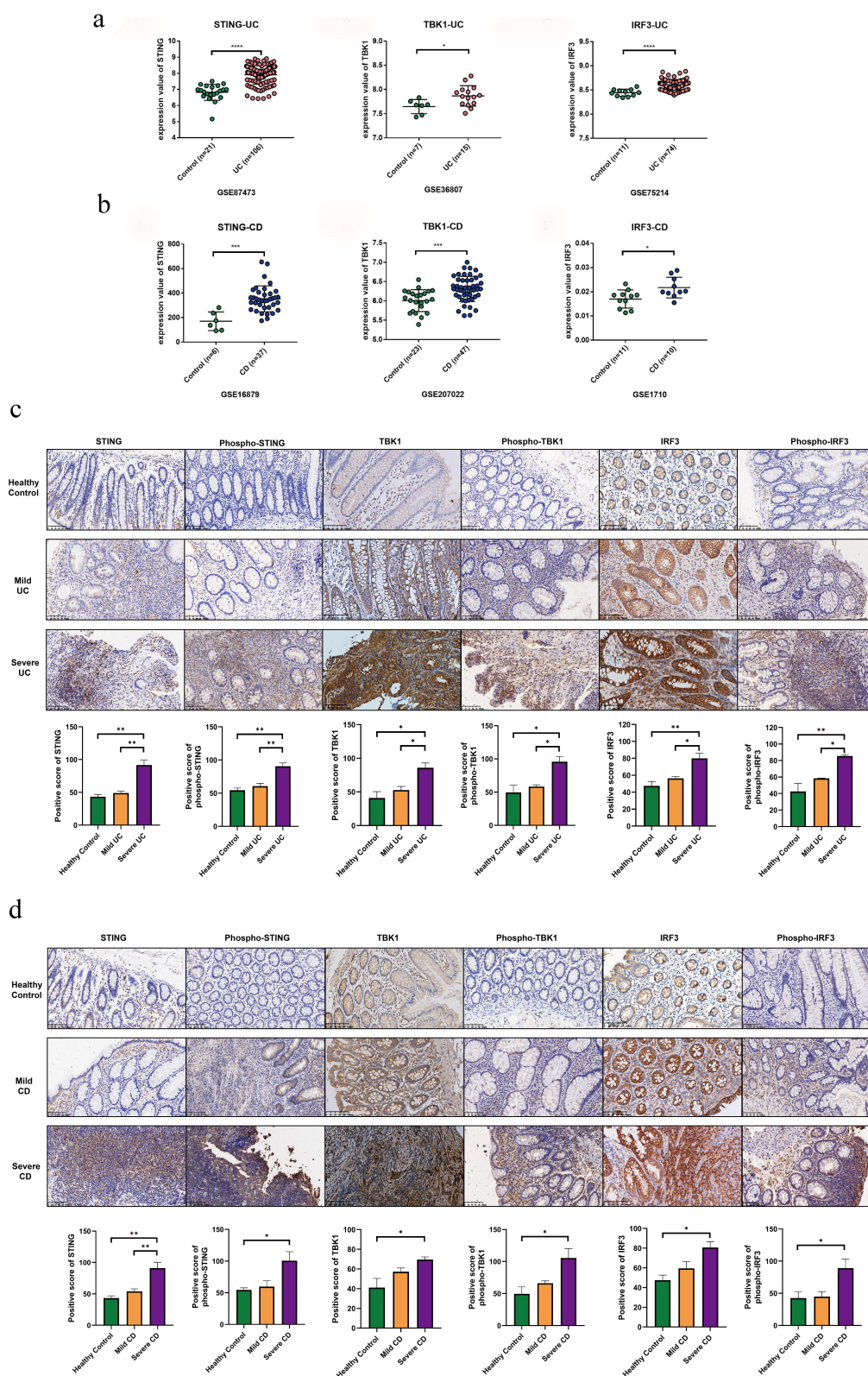
Figure 9. Activation of STING-TBK1-IRF3 pathway correlates with disease severity in IBD. (a) GEO-based analysis showing the mRNA expression of STING, TBK1 and IRF3 genes in the intestine of patients with UC. (b) GEO-based analysis showing the mRNA expression of STING, TBK1 and IRF3 genes in the intestine of patients with CD. (c) IHC assay revealed differences in the expression of STING, phospho-STING, TBK1, phospho-TBK1, IRF3 and phospho-IRF3 proteins in colons of the control, mild UC and severe UC patients. (d) IHC assay showed differences in the expression of STING, phospho-STING, TBK1, phospho-TBK1, IRF3 and phospho-IRF3 proteins in colons of the control, mild CD and severe CD patients. All of the above IHC experiments contained three biological replicates. Data were shown as mean ± SEM. (a, b) Statistical significance was assessed by unpaired Student's t test; (c, d) statistical significance was assessed by one-way ANOVA with Tukey's multiple comparisons test. *$p \leq 0.05$, **$p \leq 0.01$, ***$p \leq 0.001$.

expression of above proteins in the intestine of UC and CD patients tended to increase gradually with disease severity. Especially for UC patients, the expression of STING-TBK1-IRF3 pathway proteins differed markedly between mild and severe UC. Therefore, it is conceivable that patients with severe IBD who have significant STING activation in the gut, especially those with UC, could benefit more from FMT therapy, in line with the findings of a recently published meta-analysis.[15]

Discussion

It is accepted that the pathogenesis of IBD is an abnormal and overactive immune response of genetically susceptible individuals to the commensal microbiota in the gut under the influence of a harmful environment. Because of the direct targeting on the disturbed gut microbiota, which is closely related to the pathogenesis of IBD, FMT has been considered as a promising novel therapy for the disease in recent years.[37] However, the individual variability in the efficacy of this therapy is an issue of concern, which is speculated to correlate with the colonization of the donor microbiota in the recipients' intestine.[5] Here, we revealed that FMT provides treatment for colitis in a STING-dependent manner. Mechanistically, STING enhanced the negatively modulating effect of FMT on pro-inflammatory immune cells and facilitated the overall colonization of healthy donor-derived microbiota, mainly probiotic *Lactobacillales*, in the recipients' gut. These findings identified an important role for STING during the FMT treatment of colitis and highlighted the prospects of targeting STING to optimize FMT therapy.

According to the results of the HPA database analysis, we confirmed the widespread expression of STING in a variety of cells, as illustrated in Figure 1 (a),(b). However, based on single-cell sequencing analysis, STING was significantly enriched in immune cells, especially macrophages. Accumulation of STING in intestinal myeloid cells, particularly intestinal macrophages, has been proved to trigger the T cell-dependent inflammatory response and to be the initial driver of intestinal inflammation.[10] Moreover, our study further demonstrated that in the state of intestinal inflammation, STING-activated macrophages tend to produce more pro-

inflammatory cytokines by promoting the differentiation of M1 macrophages through the GM-CSF /STAT5 signaling pathway, which partly explained the promotion of intestinal inflammation by STING, in line with Martin et all.[11] Interestingly, however, STING knockout mice also developed severe colonic inflammation in response to DSS. On the basis of the findings by Zhu Q and Yu Y et al.,[38,39] our studies further revealed that STING$^{-/-}$ mice exhibited poor integrity of the intestinal mucosal barrier, which may account for the increased susceptibility to DSS due to STING deficiency. Accordingly, STING acts as "a double-edged sword" in colitis, which is related to the differential expression and diverse biological functions of STING in colonic cell subsets.

Notably, although STING plays a bi-directional role in colitis, our findings revealed for the first time that only colitis mice with high STING expression benefit most from FMT therapy, as evidenced by significant improvements in survival, weight loss, colon length, DAI and HI score, etc. Mechanistically, we concentrated on the differential alterations in immune cell subsets as well as intestinal bacteria between the FMT-treated and untreated groups in the context of different STING expression.

Th1 cells, as the major subset of CD4$^+$ T cells, are closely associated with the pathogenesis of IBD. In colonic inflammation, splenic Th1 cells migrate to the inflamed intestine via peripheral blood or lymphatic circulation in response to intestinal mucosal chemokines,[40] and act together with intestine-derived Th1 cells that are differentiated from resident-memory CD4$^+$ T cells.[41] Th1 cells stimulate a feed-forward cycle of inflammatory response by inducing apoptosis of intestinal epithelial cells, releasing large amounts of pro-inflammatory cytokine such as IFN-γ, TNF-β and TNF-α, and promoting the expression of cell adhesion molecules in the intestinal mucosa to recruit more immune cells, etc.[42] Based on our results, activation of STING promoted the downregulation of Th1 cells in spleen, MLN and LP by FMT, respectively, thereby comprehensively blocking the induction of cascade inflammatory responses.

Unlike Th1 cells, intestinal Th17 cells exhibit a higher tissue-specific profile, presenting a more active state than in the spleen or MLN.[43] Inflammatory Th17 cells, mainly IL-17A$^+$ cells, are significantly enriched in the intestinal mucosa

of IBD patients and animal models, where they are co-activated by IL-6, IL-23 and IL-1β, and recruit immune cells to exacerbate colitis by secreting inflammatory cytokines.[23] In addition, Th17 cells can also differentiate into Th1 and Th2 phenotypes to synergize their pro-inflammatory effects.[42,44] In this experiment, only the STING overexpressed group of colitis mice showed a significant down-regulation of pathogenic Th17 cells in the intestinal mucosa compared with the untreated group after FMT therapy, suggesting that STING assists FMT in negatively regulating the differentiation of Th17 cells, thereby alleviating intestinal inflammation.

Th1/Th2 ratio, as a hallmark of immune homeostasis *in vivo*, is intimately associated with the development and progression of IBD.[45,46] In the absence of FMT treatment, the splenic Th1/Th2 ratio, which represents the overall immune homeostasis of the body, was remarkably higher in both the STING$^{-/-}$ and STING-activated groups, positively correlating with the severity of colitis. Interestingly, after FMT treatment, an obvious downregulation of splenic Th1/Th2 ratio in the STING-activated mice was observed despite the concomitant decrease in both Th1 and Th2 cells. This implicates that STING assists FMT therapy to improve the impaired immune homeostasis in colitis.

Intestinal macrophages, as the bridge connecting innate and adaptive immunity, are key players in the development and progression of IBD.[47] Macrophages accumulate abundantly in the inflamed gut during the active stage of IBD and release multiple pro-inflammatory factors upon recognition of pathogen-associated molecular patterns (PAMPs), promoting the activation of various effector T cells, including Th1 and Th17.[48] Intestinal macrophages mainly include two polarization phenotypes, the pro-inflammatory M1-like phenotype and the anti-inflammatory M2-like phenotype. These two phenotypes are in a dynamic polarization process, and hyperpolarization of the M1 phenotype has been proved to be a pathological feature of IBD.[25] After FMT treatment, the percentage of intestinal macrophages and the M1/M2 ratio were significantly reduced in the SITNG-overexpressing group, indicating that STING enhanced the role of FMT in promoting the polarization of M1 type macrophage to M2 type

macrophage, thereby contributing to the alleviation of colonic injury.

Next, we sought to explain the mechanism by which STING enhances the negative regulation of inflammatory immune cells by FMT. Considering that dysregulated gut microbes are the key features of IBD and the main therapeutic targets of FMT, we focused on the effect of STING on the colonization of transplanted bacteria.[49] According to our results, healthy donor-derived microbiota, mainly probiotic *Lactobacillales*, colonize the recipients' gut in a STING-dependent manner, thereby maximizing the efficacy of FMT.

Lactobacillales, an order belonging to the phylum Firmicute, is a group of Gram-positive bacteria that can produce large amounts of lactic acid from fermentable carbohydrates. Several groups of bacteria belonging to the *Lactobacillales* have been found to be closely associated with the remission of colitis, including *Lachnospiraceae*,[50] *Ligilactobacillus*,[51] and *Lactobacillus*,[52] etc. In particular, *Ligilactobacillus*, whose colonization in the recipients' gut was closely correlated with STING expression, has been shown to facilitate the recovery of the gut microbiota and the intestinal barrier function in mice with colitis.[53] In addition, it was also demonstrated that *Ligilactobacillus* could alleviate DSS-induced colitis in mice by synergizing with the environmental sensor mammalian aryl hydrocarbon receptor (AHR) and tryptophan metabolism pathway.[51] Moreover, the enhanced adhesion of probiotic *Lactobacillales* to the intestinal epithelium can reduce the ecological niches of pathogenic bacteria as well. In contrast, *Allobaculum*, which degrades protective mucins in the intestinal mucosa and induces the proliferation of inflammatory Th17 cells, has been demonstrated to cause an increased susceptibility of the intestine to DSS-induced colitis.[54] Among the FMT-treated groups, the abundance of *Allobaculum* gradually decreased with the increasing expression of STING, suggesting that STING may assist donor-derived probiotics to displace the ecological niches of certain pathogenic bacteria during FMT therapy, thereby reducing the colonization of the inflamed gut by pathogenic bacteria.

We further explored the potential mechanisms by which STING affects the colonization of *Lactobacillales*. The results revealed that CD14 was

significantly overexpressed in intestinal epithelial cells co-cultured with STING-activated macrophages. Notably, CD14, as a glycosylphosphatidylinositol-anchored protein, is expressed not only in immune cells such as monocytes, macrophages and dendritic cells, but also in nonimmune cells such as epithelial cells.[55,56] As a matter of fact, CD14 on intestinal epithelial cells is able to bind with high affinity to the adhesin LTA of *Lactobacillales*, thereby promoting their adhesion.[57] It has been reported that LTA of *Lactobacillales* binding to CD14 antagonizes the inflammatory damage caused by pathogenic bacteria,[58,59] which may be one of the reasons why STING improves the efficacy of FMT.

In addition to the colonization abundance of gut microbes, it is well recognized that certain specific metabolites from the gut microbiota are also essential in mediating host-microbe crosstalk.[52] Consistent with alterations in the composition of intestinal microbiota, changes in specific gut metabolome after FMT therapy were also correlated with the expression of STING, including metabolic pathways of fatty acid and tetracycline biosynthesis. Short-chain fatty acids (SCFAs), as the major components of fatty acids, have been shown to play an important role in the anti-inflammatory immune response against colitis.[3,60] In addition, SCFAs regulate the expression of epithelial genes involved in energy metabolism, support epithelial cell proliferation, enhance the colonic epithelial barrier and affect intestinal bacterial communication.[5,61,62] Similarly, tetracycline exerts its anti-inflammatory effects through specific modifications in TLR and microRNA expression, resulting in improved microbial-derived signaling and mucosal protection in intestine.[28] Therefore, anti-inflammatory metabolic pathways such as fatty acids and tetracycline biosynthesis are enriched in the gut in a STING-dependent manner during FMT therapy, contributing to maximize the efficacy of FMT.

Ultimately, since STING facilitates the efficacy of FMT in the treatment of IBD, it was asked which group of IBD patients could benefit the most from FMT therapy. Based on GEO database analysis and IHC analysis, we concluded that intestinal inflammation licenses the accumulation and activation of STING in the intestine with a tendency to increase

as the disease worsens.[10] In this regard, those IBD patients with activated STING in the gut may benefit more from FMT therapy. Therefore, considering the STING-dependent nature of FMT in the treatment of colitis, it is proposed that STING, as a key target of FMT, has the potential to be a biomarker for screening individuals most suitable for FMT therapy in order to optimize FMT treatment regimens and improve clinical outcomes.

Materials and methods

Animals

C57BL/6J mice (8–10 weeks of age, female, weighing 20.0 ± 2.5 g) were purchased from Beijing Vital River Laboratory Animal Technology Co., Ltd. STING knockout (STING$^{-/-}$) parental mice on the C57BL/6J background were provided by Prof. Zhanju Liu of Tongji University and were housed and bred at the Animal Centre of Zhengzhou University. The schematic representation of the knockout in STING$^{-/-}$ mice is shown in Supplementary Figure 7, with a total knockout gene sequence length of 560 bp. All parents of the STING$^{-/-}$ mice used in this study have been genetically identified using PCR agarose gel electrophoresis (Supplementary Figure 8). A total of 100 C57BL/6J female mice, including 70 wide-type (WT) mice as well as 30 STING-knockout (STING$^{-/-}$) mice, were used in this study. The mice used for the study were all 8–10 weeks old and weighed approximately 18-22 g. All experimental mice were housed in the Animal Center of the Second Affiliated Hospital of Zhengzhou University in an specific pathogen-free (SPF) environment with indoor temperature and humidity of 22–26°C and 40%-70%, respectively. All animal experiments in this study were approved by the Ethics Committee of the Second Affiliated Hospital of Zhengzhou University (approval number: 2022061), and were conducted in accordance with the NIH Guide for the Care and Use of Laboratory Animals.

Cells

The mouse colon cancer cell line (CT26) was provided by Prof. Yaohe Wang from Zhengzhou

University and cultured in Dulbecco's Modified Eagle Medium (DMEM) supplemented with 10% fetal bovine serum (FBS), at an incubator temperature of 37°C and a CO2 concentration of 5%. The mouse macrophage cell line (RAW264.7) also cultured in Dulbecco's Modified Eagle Medium (DMEM) supplemented with 10% fetal bovine serum (FBS), at an incubator temperature of 37°C and a CO2 concentration of 5%.

For DMXAA stimulation experiments of CT26, CT26 cells with high STING expression were obtained by stimulation with DMXAA (CAT: #S1537; Selleck) at a concentration of 50ug/ml for 24 hours. In parallel, CT26 cells from the control group were treated with DMSO, the solvent for DMXAA, for 24 hours. All cells were re-cultured for another 24 hours after the end of stimulation and then collected for the next step.

For DMXAA and/or LPS stimulation experiments of RAW264.7 cells, RAW264.7 cells were firstly pre-stimulated with DMXAA for 4 h. After pre-stimulation with DMXAA, the LPS group was added with LPS solution (1ug/ml;CAT: L4391; Sigma), and then the cells were collected for the next step after continuous co-stimulation for 20 h. Similarly, RAW264.7 cells from the control group were treated with DMSO (solvent for DMXAA) for 24 hours prior to cell collection.

For the co-culture experiments of CT26 and RAW264.7 cells, the detailed procedure has been shown in Supplementary Figure 5. Briefly, on the first day, RAW264.7 were cultured on six-well plates, and CT26 cells were cultured on sterilized round coverslips smaller than the bottom area of the upper chamber of the transwell. On the second day, DMXAA (50ug/ml) and/or LPS (1ug/ml) were sequentially added to the RAW264.7 cells in the chronological order shown in Supplementary Figure 5, and then the sterile slides with adherent CT26 cells were placed into the upper chamber of the transwell to be co-cultivated with the RAW264.7 cells for 24 hours. On the third day, the slides with adherent CT26 were removed and co-cultured with the pre-prepared *Ligilactobacillus murinus (L. murinus)* solution at a concentration of 10^7/well for 3 h. The unadherent CT26 bacteria were then rinsed with PBS, fixed with 4% paraformaldehyde (PFA), and subjected to Fluorescence in situ hybridization (FISH) assays.

Co-culture of cells and bacteria

Ligilactobaclillus murinus (*L. murinus*) were purchased from BioSci Biotech (Hangzhou, China). *L. murinus* were grown using MRS broth or plates (CAT#m8540, Solarbio, China). For the co-culture experiment of bacteria with the CT26 cells, 10 ul of the overnight culture to log phase (~10^7 bacteria) was added to the wells of a six-well plate in which sterilized round glass coverslips of CT26 were placed, and co-cultured for 3 hours at 37°C in a 5% CO2 incubator. After incubation, cells were washed three times with PBS and fixed in 4% paraformaldehyde for 15 min before being used for further assays.

Patients and samples

All participants were recruited via the Department of Gastroenterology, The Second Affiliated Hospital of Zhengzhou University. Patients were diagnosed with UC or CD according to the British Gastroenterological Society consensus guidelines[6,63] and had not been treated with medications including biologics, immunologics or steroids. Patients with UC and CD were grouped on the basis of disease severity according to Modified Mayo Disease Activity Index (MMDAI) scoring system[64] or Crohn's Disease Activity Index (CDAI) scoring system,[65,66] respectively. Intestinal biopsy samples were obtained from all enrolled patients with UC or CD. The control group was selected from normal tissue that originated at least 5 cm away from the tumor site in surgically removed colon from patients with colorectal cancer.

Genomic DNA extraction and PCR assays for the genetic testing of STING knockout mice

Toes of STING$^{-/-}$ mice and WT mice were clipped for genotype identification, which was carried out using the One Step Mouse Genotyping Kit (CAT: PD101–01; Vazyme). Proteinase K and 1×Mouse Tissue Lysis Buffer were mixed to make 1×Mouse Tissue Lysis Solution for the extraction of total DNA. Then, the target gene fragments were amplified by PCR according to the kit instructions. The primers for STING were as follows: Forward primer, 5′-

TTTACAACCTCACCGACTT-3'; Reverse primer, 5′- CATGCTTAGGGACTTATAGAG-3'. The molecular weight of the amplified product was analyzed by agarose gel electrophoresis.[67]

Multi-immunofluorescence assay

The three immunofluorescence markers, in the Multi-immunofluorescence assay, namely STING (CAT: #13647S; Cell Signaling technology), CD45 (Cat: GB113886–100; Servicebio) and EpCAM (Cat: GB11274–100; Servicebio), are mainly based on the Telamid Signal Amplification (TSA) technique. The main principle of the technique is that fluorescently labeled tyramine becomes activated tyramine under the action of HRP and H2O2, and adheres to the protein tyrosine residues around the target. The binding was covalent, while the binding between the primary antibody and the target and the second antibody and the primary antibody was non-covalent. The first round of the primary antibody and the second antibody were eluted by microwave repair treatment, and the fluorescently labeled tyramine remained attached around the target. When detecting the second target, it is equivalent to a new round of labeling, without considering whether the antibodies of the second round cross-react with the antibodies of the first round. The procedure was as follows: after deparaffinize, rehydrate, antigen repair and serum blocking of paraffin sections, the first primary antibody was added, followed by the HRP-labeled secondary antibody of the corresponding species; next, microwave treatment was carried out, and serum blocking was carried out again, and the second primary antibody was added in turn, and so on. Finally, the nuclei were restained with DAPI, and the images were captured after sealing.

Single-cell RNA sequencing (scRNA-seq)

Mouse total colon cells from the WT mice with DSS-induced colitis were isolated by tissue dissociation and FACS purification prior to DNBelab C4 scRNA-seq. There were three replicates. After construction of the oligo library, the cDNA was fragmented, end repaired and added A-tailing of cDNA Products. After completion of adaptor Ligation and PCR amplification of cDNA products, library quality control was performed. The cDNA and Oligo Products were subjected to circularization and then sequenced. Single-stranded circle DNA molecules are replicated via rolling cycle amplification, and a DNA nanoball (DNB) which contain multiple copies of DNA is generated. Sufficient quality DNBs are then loaded into patterned nanoarrays using high-intensity DNA nanochip technique and sequenced through combinatorial Probe-Anchor Synthesis (cPAS).

Single-cell RNA sequencing analysis

Single-cell data of control WT mice without DSS-induced colitis used in this study were downloaded from the public gene expression omnibus (GEO) database of the National Center for Biotechnology Information (NCBI) under GSE211578. Data processing includes batch correction, doublet removal, cell clustering and cell annotation. Barnes-Hut t-distributed Stochastic Neighbor Embedding (t-SNE) analysis was run for visualization using the Seurat R toolkit. Expression of STING in each cellular subset was visualized in markerScatter plots. All bioinformatics analysis was performed using R version 3.4.0 (R Foundation, https://www.rproject.org.)

Western Blot assay

Proteins from mouse colon tissues, CT26 and RAW264.7 cells were extracted using RIPPA lysate containing protease inhibitor and phosphatase inhibitor cocktail. After the protein concentration was assessed using the BCA Protein Assay Kit (CAT: CW0014S, CoWin), protein samples were subjected to SDS polyacrylamide gel electrophoresis and were transferred to polyvinyl difluoride membranes. The membranes was blocked with BSA blocking solution (CAT: CW0054S, CoWin) for 1 hour and then incubated with the primary antibodies, including anti-STING (1:1000 dilution) (CAT: #13647S, Cell Signaling technology), anti-pSTING (1:1000 dilution) (CAT: #72971S, Cell Signaling technology), anti-TBK1 (1:500 dilution) (CAT: ab40676, Abcam), anti-pTBK1 (1:1000 dilution) (CAT: ab186469, Abcam), anti-IRF3 (1:1000 dilution) (CAT: #4302S, Cell Signaling technology), anti-pIRF3 (1:1000 dilution) (CAT: #4947S,

Cell Signaling technology), anti-GM-CSF (1:1000 dilution) (CAT:17762-1-AP, Proteintech), anti-pSTAT5 (Tyr694) (1:1000 dilution) (CAT:#4322, Cell Signaling technology), and beta-Actin (1:2000 dilution) (CAT: #4970S; Cell Signaling technology). Subsequently, the membranes were washed and incubated with horseradish peroxidase-conjugated anti-rabbit or anti-mouse secondary antibody. Protein bands were visualized by using eECL Western Blot Kit (CAT: CW0049S; CoWin) and were exposed with GE Amersham Imager 600 (General Electric Company).

Design of animal experiments

Based on the timing of the experimental endpoints, the animal experiments involved in this study were categorized into two parts: Therapeutic Efficacy Experiment and Mechanism Experiment. This two types of study were conducted independently of each other. Therapeutic Efficacy Experiments lasted for 3 months, which included the time required to observe the survival of the mice and to collect their feces after the drug intervention; in the Mechanism Experiment, the animal treatment portion lasted for 12 days, which included only the time required for the drug intervention.

The mice involved in both the Therapeutic Efficacy Experiment and Mechanism Experiment were categorized into 3 categories: STING knock-out mice (STING$^{-/-}$), wild-type mice (WT), and STING-actived mice obtained by intraperitoneal injection of DMXAA at a dose of 10 mg/kg/day for 7 days.

In terms of experimental grouping, the Therapeutic Efficacy Experiment and Mechanism Experiment were grouped in the same way, with six experimental groups (Figure 3(b)). That is, three colitis model groups (STING$^{-/-}$+DSS, WT+DSS, DMXAA+DSS) that were only administered 2% dextrose sodium sulfate (DSS) in drinking water, as well as three therapeutic groups that were combined with fecal microbiota transplantation (FMT) therapy in DSS-induced colitis (STING$^{-/-}$+DSS+FMT, WT+DSS+FMT, DMXAA+DSS+FMT). Notably, in the Therapeutic Efficacy Experiment, there were 12 mice in each group, totaling 72 mice; while in the Mechanism Experiment, there were 3 mice in each group, totaling 18 mice. The remaining 10 WT mice did not receive any pharmacological intervention in order to provide fresh and healthy feces.

The drug treatments for the Therapeutic Efficacy Experiment were the same as those for the Mechanism Experiment. First, mice in each group were orally administered 2% DSS from day 0 to day 10 of the experiment to develop the classical mouse model of colitis. Next, on days 5–12 of the experiment, mice in each of the three FMT groups were gavaged with the healthy bacterial solution at a dose of 200ul/day/mouse to mimic the clinical FMT therapeutic pattern (Figure 3(a)). Meanwhile, mice in the non-FMT groups were treated with the same dose of Ringer's solution as a control. Fresh transplant material used in FMT was derived from healthy WT mice of the same age.

During the Therapeutic Efficacy Experiment, the body weight, stool consistency and rectal bleeding status of mice in each group were assessed daily from day 0 for Disease Activity Index (DAI) scoring. Meanwhile, feces were collected from each experimental mouse and stored at −80°C for subsequent 16SrDNA assays. In addition, the survival of mice in each group was also recorded until day 90 of the experiment, and then the survival curve was plotted. At the end of the Therapeutic Efficacy Experiment, all mice were euthanized. In the Mechanism Experiment, all mice were euthanized on day 12 after the end of DSS and FMT treatments. The mice were dissected, their colons were isolated, and the length of the colons in each group were measured and photographed. After rinsing the isolated colon with PBS, a portion of colon tissue was cut and fixed with 4% paraformaldehyde solution, followed by paraffin embedding and HE staining. Meanwhile, 0.5-mm-sized colon tissues were cut and kept in Trizol solution for RT-qPCR experiments to detect the expression of inflammatory factors TNFα, and IL-6 in each group of mice. In addition, cells from the remaining colon tissues, mesenteric lymph nodes and spleens of each group of experimental mice were extracted for Flow Cytometry to assess the percentage of immune cells such as T helper (Th)1, Th2, Th17 cells and macrophages.

Colitis induction and assessment of disease severity

To induce acute experimental colitis, mice were administered 2% (w/v) dextran sodium sulfate (DSS, molecular weight, 36–50 kDa; MP Biomedicals) in their drinking water for 10 days. During the experimental period, all mice with colitis were monitored for weight lose, fecal morphology and blood in stool to assess the disease activity index (DAI). The detailed scoring criteria are as follows, weight loss (0 points = 0% weight loss from baseline; 1 point = 1–5% weight loss; 2 points = 5–10% weight loss; 3 points = 10–20% weight loss; and 4 points = more than 20% weight loss); rectal bleeding (0 points = negative; 2 points = positive hemoccult test; and 4 points = visible bleeding); and stool consistency (0 points = normal feces; 1 point = loose stool; 2 points = watery diarrhea; 3 points = slimy diarrhea, little blood; and 4 points = severe watery diarrhea with blood. The rectal bleeding was detected by the Fecal Occult Blood Test Kit (CAT: TC0513; Leagene). The sum of the scores for the three indicators above is the total DAI score, with a maximum score of 12. For mice used for survival, body weight and DAI analysis (n = 12), the survival of mice in each group was recorded up to day 90 to plot the survival curve; and the body weight and DAI changes of mice in each group were recorded up to day 12 to plot the body weight and DAI curve. Mice used for mechanism experiments, including Histological Assessment, Immunohistochemistry and Flow cytometry Assay, were sacrificed on day 12 of the experiment (n = 3).

Acquisition of FMT materials and treatment process

Fresh feces from 10–12 age- and sex-matched healthy mice were collected daily (in autoclaved EP tubes using sterile swabs) and homogenized in sterile pre-cooled PBS, and the above fluids were filtered using a 70um filter to obtain a scum-free bacterial solution at a concentration of 50 mg/ml. From day 5 to day 12 of DSS treatment, FMT was administered by forced gavage at a dose of 200ul/mouse/day. Considering the possible effect of gastric acid on the transplanted intestinal microbiota, the sodium bicarbonate solution (0.084 g/ml) was given at a dose of 200 ul/mouse/day 10–20 min

before gavage to neutralize the gastric acid, and the control mice were given the same volume of sterile Ringer's solution.

Histological assessment

Colonic tissues was fixed by 4% paraformaldehyde, embedded in paraffin, and sections of paraffin were stained with hematoxylin and eosin (H&E). Using light microscopy, colonic sections (5 μm) were evaluated by an experienced pathologist in a blinded manner according to a scoring criteria. The pathology scoring criteria was graded based on the following parameters: Inflammatory cell infiltrate, which was evaluated by the number of leukocyte: 0 point = no significant change, 1- mild, infiltrated leukocytes in focal or occasional, 2 points = moderate, infiltrated leukocytes with more than one focus and 3 points = severe, infiltrated leukocytes diffuse or continuous; Extent of involvement: 1 point = covering 1–25%, 2 points = covering 26–50%, 3 points = covering 51–75%, and 4 points = covering 76–100% of the intestinal mucosal surface; Depth of intestinal mucosal disruption: 0 point = no disruption existed, 1 point = disruption reaching the submucosa, 2 points = disruption reaching the muscular layer, 3 points = disruption reaching the plasma membrane layer; Crypt damage: 0 point = intact crypt, 1 point = loss of the basal third of the crypt, 2 points = loss of two-thirds of the crypt, 3 points = loss of the entire crypt with the surface epithelium remaining intact, and 4 points = loss of the entire crypt and surface epithelium (erosion).[10,68]

Quantitative real-time (qRT)-PCR assay

Total RNA of colonic tissues from mice were extracted using TRIzol reagent (CAT: CW0580S, CoWin), along with testing their concentration and purity for quality assurance. RNA was then used as a template to form complementary DNA (cDNA) by reverse transcription, which is performed using the HiScript III All-in-one RT SuperMix Perfect for qPCR Kit (CAT: R333; Vazyme) based on the manufacturer's instructions. Primer sequences of TNF-α, IL-6 and Occludin were designed by Sangon Biotech (https://www.sangon.com/) and

synthesized in Sango Biotech. qRT-PCR was performed in the ABI StepOnePLus system (Applied Biosystems) using a Taq Pro Universal SYBR qPCR Master Mix Kit (CAT: Q712–02; Vazyme). The relative expression levels of target genes were normalized to GAPDH, and calculated by the $2^{-\Delta\Delta CT}$ algorithm. Primer sequences are detailed in Supplementary Table 1.

Flow cytometry assay

Cells from lamina propria (LP), mesenteric lymph nodes (MLN) and spleen were stained with Zombie NIR APC/Cy7 (CAT: 423105; Biolegend) for the identification of live cells, and with anti-CD4 FITC (CAT: 100406; Biolegend), anti-F4/80 Brilliant Violet 605 (CAT: 123133; Biolegend), anti-CD11b PerCP/Cyanine5.5 (CAT: 101228; Biolegend) for surface labeling. For intracellular cytokine staining, 1.5×10^6 cells were cultured and stimulated in Dulbecco's modification of Eagle's medium Dulbecco (DMEM) supplemented with 10% FBS and 2% Leukocyte Activation Cocktail (CAT: 550583; BD Pharmingen™) for 4–6 hours at 37°C, 5% CO_2 cell incubator. Next, the cells were washed in PBS and then fixed and permeabilised with the Transcription Factor Buffer Set (CAT: 562574; BD Pharmingen™). The reaction was terminated with Perm/Wash buffer after 40–50 min at 4°C with protection from light. Subsequently, the cells were centrifuged and stained intracellularly with anti-IFN-gamma Brilliant Violet 650 (CAT: 505832; Biolegend), anti-IL-4 PE/Cyanine7 (CAT: 504118; Biolegend), anti-IL-17A Brilliant Violet 421 (CAT: 506926; Biolegend), anti-NOS2 (iNOS) PE (CAT: 696806; Biolegend), anti-CD206 (MMR) APC (CAT: 141708; Biolegend). All Cells were acquired on the Agilent NovoCyte technology (ACEA NOVOCYte3130). Flow cytometry analysis was done with the FlowJo software.

16S rDNA gene amplicon sequence libraries and data analysis

The genomic DNA of the fecal samples (five biological replicates per group) were extracted by CTAB method. The quality of the extracted DNA was examined using agarose gel electrophoresis, while the extracted DNA was quantified by UV spectrophotometer. Polymerase chain reaction (PCR) was used to amplify the higher-variable region (V3-V4) of bacterial 16S ribosomal DNA. The PCR primers were designed against the conserved region to target the variable region of the 16S/ITS2 rDNA gene. The forward barcoded primers were targeted to the V3 region (v3f_341f-CCTACGGG NGGCWGCAG) and reverse primer were targeted to the V4 region (v4r_806r-GGACTACN VGGGTWTCTAAT). PCR amplification products were detected by 1.5% agarose gel electrophoresis.

The target fragments were recovered using the AxyPrep PCR Cleanup Kit. After purification of the PCR products using the Quant-iT PicoGreen dsDNA Assay Kit, the library was quantified on the Promega QuantiFluor fluorescence quantification system. Afterward, the pooled library was loaded on Illumina platform using a paired-end sequencing protocol (2×250 bp).

Paired-end reads was assigned to samples based on their unique barcode and truncated by cutting off the barcode and primer sequence. Paired-end reads were merged using FLASH (v1.2.8) (for 16S)/PEAR (v0.9.6) (for ITS2). Quality filtering on the raw reads were performed under specific filtering conditions to obtain the high-quality clean tags according to the fqtrim (v0.94). Chimeric sequences were filtered using Vsearch software (v2.3.4). ASV feature sequences and abundance tables were obtained by denoising the valid tags using the Divisive Amplicon Denoising Algorithm 2 (DADA2). Alpha diversity and Beta diversity were analyzed by QIIME2 process, and pictures were drawn by R (v3.5.2). The sequence alignment of species annotation was performed by Blast, and the alignment database was SILVA and NT-16S. Significant differences between groups were analyzed using the linear discriminant analysis effect size (LEfSe) algorithm, which was performed using the OmicStudio tools (https://www.omicstudio.cn.) with a default linear discriminant analysis (LDA) score threshold set to 3. Functional predictions of the microbiota were made with PICRUSt2 (https://www.omicstudio.cn/tool), which enabled the prediction of bacterial and archaeal metabolic functions by comparing existing 16S rDNA gene sequencing data with the Kyoto Encyclopedia of Genes and Genomes (KEGG)

database. Correlation analysis were performed to identify the relationship between metabolic pathways and microbiota using the OmicStudio tools at https://www.omic-. studio.cn/tool.

Fluorescence in situ hybridization (FISH)

Round coverslips of CT26 cells fixed by 4% paraformaldehyde were digested with proteinase K (20ug/ml). After prehybridization treatment, hybridization buffer (0.9 M NaCl, 20 mM Tris-HCl, 0.01% sodium lauryl sulfate, and 10% formamide; pH 7.5) containing the fluorescent probe targeting *L.murinus* was added and incubated at 40°C overnight. The samples were incubated with DAPI in PBS for 8 min at room temperature and then mounted with dropwise addition of anti-fluorescence quencher. Images were obtained on a Nikon fluorescence microscope (Nikon, Tokyo, Japan).

Immunohistochemistry assay

Immunohistochemistry (IHC) was performed on colon samples from patients with IBD or mice with colitis. Formalin-Fixed Paraffin-Embedded (FFPE) colon tissues were sectioned into slices (5 μm) and mounted to glass slides. Tissue sections were dewaxed, rehydrated, and subjected to the antigen retrieval in microwave with EDTA citrate buffer (pH = 7.8) (CAT: C1032; Solarbio). Slides were then blocked with Normal Goat Serum (CAT: SL038; Solarbio) prior to the staining. The sections were incubated with antibodies specific for STING (1:500 dilution) (CAT: #13647; Cell Signaling technology), phospho-STING (1:200 dilution) (CAT: PA5–105674; Invitrogen),TBK1 (1:600 dilution) (CAT: ab40676; Abcam), phospho-TBK1 (1:200 dilution) (CAT: PA5–105919; Invitrogen), IRF3 (1:200 dilution) (CAT: #4302; Cell Signaling technology) and phospho-IRF3 (1:200 dilution) (CAT: AF2436; Affinity) at 4°C overnight. After washing with PBS/Tween20 buffer (pH = 7.6), the sections were detected using an anti-rabbit secondary antibody for half an hour at room temperature, respectively. Reactions were revealed by a DAB Chromogenic Reagent Kit (CAT: abs9210; Absin). Then the intensity of staining was observed by a microscope (Leica DMi8) and analyzed by ImageJ Java. Positive scores were assessed as follows.

Firstly, three fields of view were randomly selected from each slide, and the high positive score, positive score, low positive score and negative score were calculated for each field of view based on the IHC profiler plugin;[69] then the average of each positive area was calculated; finally, the total positive score was evaluated according to the following formula: Total positive score = (high positive score × 3) + (positive score × 2) + (low positive score × 1) + (negative score × 0).

GEO database analysis

Gene expression microarrays for UC and CD patients were downloaded from the public gene expression omnibus (GEO) database of the National Center for Biotechnology Information (NCBI) under GSE87473, GSE36807, GSE75214, GSE16879, GSE207022 and GSE1710, respectively. The GSE87473 dataset contains intestinal tissue specimens from 106 UC patients and 21 healthy controls, with sequencing performed on the GPL13158 platform; the GSE36807 dataset contains intestinal tissue specimens from 15 UC patients and 7 healthy controls, with sequencing performed on the GPL570 platform; the GSE75214 dataset contains intestinal tissue specimens from 74 UC patients and 11 healthy controls, with sequencing performed on the GPL6244 platform; the GSE16879 dataset contains intestinal tissue specimens from 37 CD patients and 6 healthy controls, with sequencing performed on the GPL570 platform; the GSE207022 dataset contains intestinal tissue specimens from 47 CD controls and 23 healthy controls, with sequencing performed on the GPL13158 platform; and the GSE1710 dataset contains intestinal tissue specimens from 10 CD patients and 11 healthy controls, with sequencing performed on the GPL284 platform. The GEO2R software (https://www.ncbi.nlm.nih.gov/geo/geo2r/.) was used to analyze the differential mRNA expression of STING, TBK1 and IRF3 between IBD patients and healthy controls. In detail, differential genes were screened based on adjusted P-values <0.05 and |log$_2$ (Fold Change) | >1. Subsequently, mRNA expression of STING, TBK1 and IRF3 in colon tissues from healthy control or UC patient or CD patient was identified by the probe ID numbers of the screened differential genes, respectively.

Statistical analysis

Data were analyzed and plotted using GraphPad Prism 8.0 software (La Jolla, CA, USA). Data that conformed to a normal distribution were expressed as mean ± SEM. For the analysis of microbiome, data transformation is employed to achieve a normal distribution (logarithm, square root, inverse and inverse logarithm) if required and possible. Comparisons between two groups were made using two-tailed unpaired Student's t-test or Mann-Whitney U test. Differences among multiple groups ($n \geq 3$) were analyzed using one way analysis of variance (ANOVA) or Kruskal – Wallis tests, followed by Tukey or Dunn's post-hoc tests with Holm correction, as appropriate. For the analysis of two variables among multiple groups ($n \geq 3$), two-way ANOVA with Sidal's multiple comparisons test was employed. The Kaplan-Meier method was used to draw survival curves, and log-rank test for trend was used for determining the statistical significance of the difference in Kaplan-Meier survival. Spearman correlation was calculated to evaluate the linear association between two nonparametric variables. $p < 0.05$ was considered as statistically significant, expressed as $*p < 0.05$, $**p < 0.01$, $***p < 0.001$, and $****p < 0.0001$.

Author contributions

ZZ and BF conceived and supervised this study. ZZ and BF were responsible for all aspects of study design and managed the project. DP, YY, CZ designed and conducted most of the experiments and the bioinformatics analysis. RL, ZW, YL, DW and BW did immune assays. YW and ZL participated in interpretation of some experiments and critically reviewed the manuscript. DP, ZZ and BF interpreted all results and wrote the manuscript. All authors contributed to the article and approved the submitted version.

Data availability statement

The datasets presented in this study can be found in online repositories. The names of the repository/repositories and accession number(s) can be found in the article/Supplementary Material. 16S rDNA amplicon sequencing data have been deposited under the NCBI BioProjects (https://www.ncbi.nlm.nih.gov/bioproject/) PRJNA995185. Any additional information required to reanalyze the data reported in this study will be available upon request.

Ethics statement

This study was guided by guidelines of the Declaration of Helsinki and the principle of biomedical research involving human norms of international ethics established by the WHO and CIOMS. The Ethics Committee of The Second Affiliated Hospital of Zhengzhou University approved this research (No. 2022061). The patients/participants provided their written informed consent to participate in this study. Written informed consent was obtained from the individual(s) for the publication of any potentially identifiable images or data included in this article.

ORCID

Zhe Zhang http://orcid.org/0000-0002-8973-3563
Baisui Feng http://orcid.org/0000-0001-9440-9285

References

1. Ni J, Wu GD, Albenberg L, Tomov VT. Gut microbiota and IBD: causation or correlation? Nature reviews gastroenterology & hepatology. Nat Rev Gastroenterol & Hepatol. 2017;14(10):573–584. doi:10.1038/nrgastro.2017.88.
2. Ananthakrishnan AN. Epidemiology and risk factors for IBD. Nature reviews gastroenterology & hepatology. Nat Rev Gastroenterol & Hepatol. 2015;12(4):205–217. doi:10.1038/nrgastro.2015.34.
3. Allegretti JR, Mullish BH, Kelly C, Fischer M. The evolution of the use of faecal microbiota transplantation and emerging therapeutic indications. Lancet (Lond, Engl). 2019;394(10196):420–431. doi:10.1016/S0140-6736(19)31266-8.

4. Costello SP, Hughes PA, Waters O, Bryant RV, Vincent AD, Blatchford P, Katsikeros R, Makanyanga J, Campaniello MA, Mavrangelos C. et al. Effect of fecal microbiota transplantation on 8-week remission in patients with ulcerative colitis: a randomized clinical trial. Jama. 2019;321(2):156–164. doi:10.1001/jama.2018.20046.

5. Li SS, Zhu A, Benes V, Costea PI, Hercog R, Hildebrand F, Huerta-Cepas J, Nieuwdorp M, Salojärvi J, Voigt AY. et al. Durable coexistence of donor and recipient strains after fecal microbiota transplantation. Sci (New Y, NY). 2016;352 (6285):586–589. doi:10.1126/science.aad8852.

6. Ishikawa H, Ma Z, Barber GN. STING regulates intracellular DNA-mediated, type I interferon-dependent innate immunity. Nature. 2009;461(7265):788–792. doi:10.1038/nature08476.

7. Hu Q, Zhou Q, Xia X, Shao L, Wang M, Lu X, Liu S, Guan W. Cytosolic sensor STING in mucosal immunity: a master regulator of gut inflammation and carcinogenesis. J Exp & Clin Cancer Res: CR. 2021;40 (1):39. doi:10.1186/s13046-021-01850-9.

8. Ishikawa H, Barber GN. STING is an endoplasmic reticulum adaptor that facilitates innate immune signalling. Nature. 2008;455(7213):674–678. doi:10.1038/nature07317.

9. Motwani M, Pawaria S, Bernier J, Moses S, Henry K, Fang T, Burkly L, Marshak-Rothstein A, Fitzgerald KA. Hierarchy of clinical manifestations in SAVI N153S and V154M mouse models. Proc Natl Acad Sci USA. 2019;116(16):7941–7950.

10. Shmuel-Galia L, Humphries F, Lei X, Ceglia S, Wilson R, Jiang Z, Ketelut-Carneiro N, Foley SE, Pechhold S, Houghton J. et al. Dysbiosis exacerbates colitis by promoting ubiquitination and accumulation of the innate immune adaptor STING in myeloid cells. Immunity. 2021;54 (6):1137–53.e8. doi:10.1016/j.immuni.2021.05.008.

11. Martin GR, Blomquist CM, Henare KL, Jirik FR. Stimulator of interferon genes (STING) activation exacerbates experimental colitis in mice. Sci Rep. 2019;9(1):14281. doi:10.1038/s41598-019-50656-5.

12. Ahn J, Son S, Oliveira SC, Barber GN. STING-Dependent signaling underlies IL-10 controlled inflammatory colitis. Cell Rep. 2017;21(13):3873–3884. doi:10. 1016/j.celrep.2017.11.101.

13. Canesso MCC, Lemos L, Neves TC, Marim FM, Castro TBR, Veloso ÉS, Queiroz CP, Ahn J, Santiago HC, Martins FS. et al. The cytosolic sensor STING is required for intestinal homeostasis and control of inflammation. Mucosal Immunol. 2018;11 (3):820–834. doi:10.1038/mi.2017.88.

14. Fischer JC, Bscheider M, Eisenkolb G, Lin C-C, Wintges A, Otten V, Lindemans CA, Heidegger S, Rudelius M, Monette S. et al. RIG-I/MAVS and STING signaling promote gut integrity during irradiation- and immune-mediated tissue injury. Sci Transl Med. 2017;9 (386). doi:10.1126/scitranslmed.aag2513.

15. Fang H, Fu L, Wang J. Protocol for fecal microbiota transplantation in inflammatory bowel disease: a systematic review and meta-analysis. Biomed Res Int. 2018;2018:1–11. doi:10.1155/2018/8941340.

16. Yang W, Yu T, Zhou G, Yao S, Wakamiya M, Hu H, Paessler S, Sun J, Cong Y. Intrinsic STING switches off pathogenetic programs of Th1 cells to inhibit colitis. Cellular Mol Gastroenterol Hepatol. 2023;15 (5):1161–1179. doi:10.1016/j.jcmgh.2023.01.010.

17. Chen C, Zhang Y, Tao M, Zhao X, Feng Q, Fei X, Fu Y. Atrial natriuretic peptide attenuates colitis via inhibition of the cGAS-sting pathway in colonic epithelial cells. Int J Biol Sci. 2022;18(4):1737–1754. doi:10.7150/ijbs.67356.

18. Nagenborg J, Jin H, Ruder AV, Temmerman L, Mees B, Schalkwijk C, Müller-Klieser D, Berg T, Goossens P, Donners MMPC. et al. GM-CSF-activated STAT5A regulates macrophage functions and inflammation in atherosclerosis. Front Immunol. 2023;14:1165306. doi:10.3389/fimmu.2023.1165306.

19. Li J, Li C, Zhuang Q, Peng B, Zhu Y, Ye Q, Ming Y. The evolving roles of macrophages in organ transplantation. J Immunol Res. 2019;2019:1–11. doi:10.1155/2019/5763430.

20. Jesser EA, Brady NJ, Huggins DN, Witschen PM, Ch CH, Schwertfeger KL. STAT5 is activated in macrophages by breast cancer cell-derived factors and regulates macrophage function in the tumor microenvironment. Breast Cancer Res. 2021;23(1):104. doi:10.1186/s13058-021-01481-0.

21. Cobrin GM, Abreu MT. Defects in mucosal immunity leading to Crohn's disease. Immunological Rev. 2005;206:277–295. doi:10.1111/j.0105-2896.2005.00293.x.

22. Matsuoka K, Inoue N, Sato T. et al. T-bet upregulation and subsequent interleukin 12 stimulation are essential for induction of Th1 mediated immunopathology in Crohn's disease. Gut. 2004;53(9):1303–1308. doi:10. 1136/gut.2003.024190.

23. Chen L, Ruan G, Cheng Y, Yi A, Chen D, Wei Y. The role of Th17 cells in inflammatory bowel disease and the research progress. Front Immunol. 2022;13:1055914. doi:10.3389/fimmu.2022.1055914.

24. Ruder B, Becker C. At the forefront of the mucosal barrier: the role of macrophages in the intestine. Cells. 2020;9(10):2162. doi:10.3390/cells9102162.

25. Zhang Y, Li X, Luo Z, Ma L, Zhu S, Wang Z, Wen J, Cheng S, Gu W, Lian Q. et al. ECM1 is an essential factor for the determination of M1 macrophage polarization in IBD in response to LPS stimulation. Proc Natl Acad Sci USA. 2020;117(6):3083–3092.

26. Pu D, Liu L, Wang N, Wang D, Zhang Z, Feng B. Case report: single-cell mapping of peripheral blood mononuclear cells from a patient with both Crohn's disease and isolated congenital asplenia. Front Immunol. 2022;13:959281. doi:10.3389/fimmu.2022.959281.

27. Manichanh C, Borruel N, Casellas F, Guarner F. The gut microbiota in IBD. Nat Rev Gastroenterol Hepatol. 2012;9(10):599–608. doi:10.1038/nrgastro.2012.152.

28. Garrido-Mesa J, Algieri F, Rodríguez-Nogales A, Vezza T, Utrilla MP, Garcia F, Chueca N, Rodríguez-Cabezas ME, Garrido-Mesa N, Gálvez J. et al. Immunomodulatory tetracyclines ameliorate dnbs-colitis: impact on microRNA expression and microbiota composition. Biochemical Pharmacol. 2018;155:524–536. doi:10.1016/j.bcp.2018.07.044.

29. Koido S, Ohkusa T, Kajiura T, Shinozaki J, Suzuki M, Saito K, Takakura K, Tsukinaga S, Odahara S, Yukawa T. et al. Long-term alteration of intestinal microbiota in patients with ulcerative colitis by anti-biotic combination therapy. PLOS ONE. 2014;9(1): e86702. doi:10.1371/journal.pone.0086702.

30. Millet V, Gensollen T, Maltese M, Serrero M, Lesavre N, Bourges C, Pitaval C, Cadra S, Chasson L, Vu Man TP. et al. Harnessing the Vnn1 pantetheinase pathway boosts short chain fatty acids production and mucosal protection in colitis. Gut. 2023;72 (6):1115–1128. doi:10.1136/gutjnl-2021-325792.

31. Tang MS, Poles J, Leung JM, Wolff MJ, Davenport M, Lee SC, Lim YA, Chua KH, Loke P, Cho I. et al. Inferred metagenomic comparison of mucosal and fecal micro-biota from individuals undergoing routine screening colonoscopy reveals similar differences observed during active inflammation. Gut Microbes. 2015;6(1):48–56. doi:10.1080/19490976.2014.1000080.

32. Davenport M, Poles J, Leung JM, Wolff MJ, Abidi WM, Ullman T, Mayer L, Cho I, Loke P. Metabolic altera-tions to the mucosal microbiota in inflammatory bowel disease. Inflamm Bowel Dis. 2014;20(4):723–731. doi:10.1097/MIB.0000000000000011.

33. Liu F, Smith AD, Solano-Aguilar G, Wang TTY, Pham Q, Beshah E, Tang Q, Urban JF, Xue C, Li RW. et al. Mechanistic insights into the attenuation of intestinal inflammation and modulation of the gut microbiome by krill oil using in vitro and in vivo models. Microbiome. 2020;8(1):83. doi:10.1186/s40168-020-00843-8.

34. Sakai S, Nishida A, Ohno M, Inatomi O, Bamba S, Sugimoto M, Kawahara M, Andoh A. Ameliorating effects of bortezomib, a proteasome inhibitor, on devel-opment of dextran sulfate sodium-induced murine colitis. J Clin Biochem Nutr. 2018;63(3):217–223. doi:10.3164/jcbn.18-42.

35. Spees AM, Wangdi T, Lopez CA, Kingsbury DD, Xavier MN, Winter SE, Tsolis RM, Bäumler AJ. Streptomycin-induced inflammation enhances Escherichia coli gut colonization through nitrate respiration. mBio. 2013;4(4). doi:10.1128/mBio.00430-13 .

36. Baier J, Gänsbauer M, Giessler C, Arnold H, Muske M, Schleicher U, Lukassen S, Ekici A, Rauh M, Daniel C. et al. Arginase impedes the resolution of colitis by altering the microbiome and metabolome. J Clin Investigation. 2020;130(11):5703–5720. doi:10.1172/JCI126923.

37. Imdad A, Pandit NG, Zaman M, Minkoff NZ, Tanner-Smith EE, Gomez-Duarte OG, Acra S, Nicholson MR. Fecal transplantation for treatment of inflammatory bowel disease. Cochr Datab Syst Rev. 2023;4(4): Cd012774. doi:10.1002/14651858.CD012774.pub3.

38. Zhu Q, Man SM, Gurung P, Liu Z, Vogel P, Lamkanfi M, Kanneganti T-D. Cutting edge: STING mediates protection against colorectal tumorigenesis by governing the magnitude of intestinal inflammation. J Immunol (Baltim, Md: 1950). 2014;193(10):4779–4782. doi:10.4049/jimmunol. 1402051.

39. Yu Y, Yang W, Bilotta AJ, Yu Y, Zhao X, Zhou Z, Yao S, Xu J, Zhou J, Dann SM. et al. STING controls intestinal homeostasis through promoting antimicrobial peptide expression in epithelial cells. FASEB J. 2020;34 (11):15417–15430. doi:10.1096/fj.202001524R.

40. Feagan BG, Rutgeerts P, Sands BE, Hanauer S, Colombel J-F, Sandborn WJ, Van Assche G, Axler J, Kim H-J, Danese S. et al. Vedolizumab as induction and maintenance therapy for ulcerative colitis. N Engl J Med. 2013;369(8):699–710. doi:10.1056/NEJMoa12 15734.

41. Yokoi T, Murakami M, Kihara T, Seno S, Arase M, Wing JB, Søndergaard JN, Kuwahara R, Minagawa T, Oguro-Igashira E. et al. Identification of a unique sub-set of tissue-resident memory CD4 + T cells in Crohn's disease. Proc Natl Acad Sci USA. 2023;120(1): e2204269120.

42. Cao H, Diao J, Liu H, Liu S, Liu J, Yuan J, Lin J. The pathogenicity and synergistic action of Th1 and Th17 cells in inflammatory bowel diseases. Inflamm Bowel Dis. 2023;29(5):818–829. doi:10.1093/ibd/izac199.

43. Schnell A, Huang L, Singer M, Singaraju A, Barilla RM, Regan BML, Bollhagen A, Thakore PI, Dionne D, Delorey TM. et al. Stem-like intestinal Th17 cells give rise to pathogenic effector T cells during autoimmunity. Cell. 2021;184(26):6281–98.e23. doi:10.1016/j.cell.2021. 11.018.

44. Annunziato F, Cosmi L, Santarlasci V, Maggi L, Liotta F, Mazzinghi B, Parente E, Filí L, Ferri S, Frosali F. et al. Phenotypic and functional features of human Th17 cells. The J Exp Med. 2007;204 (8):1849–1861. doi:10.1084/jem.20070663.

45. Zenewicz LA, Antov A, Flavell RA. CD4 T-cell differ-entiation and inflammatory bowel disease. Trends Mol Med. 2009;15(5):199–207. doi:10.1016/j.molmed.2009. 03.002.

46. Lv QK, Liu JX, Li SN, Gao Y-J, Lv Y, Xu Z-P, Huang B-X, Xu S-Y, Yang D-X, Zeng Y-L. et al. Mycophenolate mofetil modulates differentiation of Th1/Th2 and the secretion of Cytokines in an active Crohn's disease mouse Model. IJMS. 2015;16 (11):26654–26666. doi:10.3390/ijms161125985.

47. Pan X, Zhu Q, Pan LL, Sun J. Macrophage immunome-tabolism in inflammatory bowel diseases: from patho-genesis to therapy. Pharmacol & Ther. 2022;238:108176. doi:10.1016/j.pharmthera.2022.108176.

48. Hegarty LM, Jones GR, Bain CC. Macrophages in intestinal homeostasis and inflammatory bowel

disease. Nat Rev Gastroenterol Hepatol. 2023;20 (8):538–553. doi:10.1038/s41575-023-00769-0.

49. Kostic AD, Xavier RJ, Gevers D. The microbiome in inflammatory bowel disease: current status and the future ahead. Gastroenterology. 2014;146 (6):1489–1499. doi:10.1053/j.gastro.2014.02.009.

50. Wang Y, Spatz M, Da Costa G, Michaudel C, Lapiere A, Danne C, Agus A, Michel M-L, Netea MG, Langella P. et al. Deletion of both dectin-1 and dectin-2 affects the bacterial but not fungal gut microbiota and susceptibility to colitis in mice. Microbiome. 2022;10(1):91. doi:10.1186/s40168-022-01273-4.

51. Fei Y, Zhang S, Han S, Qiu B, Lu Y, Huang W, Li F, Chen D, Berglund B, Xiao H. et al. The role of dihydroresveratrol in enhancing the synergistic effect of Ligilactobacillus salivarius Li01 and resveratrol in ameliorating colitis in mice. Res (Wash, DC). 2022;2022:9863845.

52. Liu Y, Zhang H, Xie A, Sun J, Yang H, Li J, Li Y, Chen F, Mei Y, Liang Y. Lactobacillus rhamnosus and L plantarum combination treatment ameliorated colitis symptoms in a mouse Model by altering intestinal microbial composition and suppressing inflammatory response. Mol Nutr Food Res. 2023;67(11):e2200340.

53. Yao M, Lu Y, Zhang T, Xie J, Han S, Zhang S, Fei Y, Ling Z, Wu J, Hu Y. et al. Improved functionality of Ligilactobacillus salivarius Li01 in alleviating colonic inflammation by layer-by-layer microencapsulation. NPJ Biofilms Microbiomes. 2021;7(1):58. doi:10.1038/s41522-021-00228-1.

54. van Muijlwijk Gh, van Mierlo G, Jansen P, van Muijlwijk GH, van Mierlo G, Vermeulen M, Bleumink-Pluym NMC, Palm NW, van Putten JPM, de Zoete MR. Identification of allobaculum mucolyticum as a novel human intestinal mucin degrader. Gut Microbes. 2021;13(1):1966278.

55. Sharygin D, Koniaris LG, Wells C, Zimmers TA, Hamidi T. Role of CD14 in human disease. Immunology. 2023;169(3):260–270. doi:10.1111/imm.13634.

56. Funda DP, Tucková L, Farré MA, Iwase T, Moro I, Tlaskalová-Hogenová H. CD14 is expressed and released as soluble CD14 by human intestinal epithelial cells in vitro: lipopolysaccharide activation of epithelial cells revisited. Infect Immun. 2001;69(6):3772–3781. doi:10.1128/IAI.69.6.3772-3781.2001.

57. Ginsburg I. Role of lipoteichoic acid in infection and inflammation. Lancet Infect Dis. 2002;2(3):171–179. doi:10.1016/S1473-3099(02)00226-8.

58. Kim HG, Lee SY, Kim NR, Ko MY, Lee JM, Yi T-H, Chung SK, Chung DK. Inhibitory effects of lactobacillus plantarum lipoteichoic acid (LTA) on staphylococcus aureus LTA-induced tumor necrosis factor-alpha production. J Microbiol Biotechnol. 2008;18 (6):1191–1196.

59. Kim JY, Kim H, Jung BJ, Kim NR, Park JE, Chung DK. Lipoteichoic acid isolated from lactobacillus plantarum suppresses lps-mediated atherosclerotic plaque inflammation. Mol Cells. 2013;35(2):115–124. doi:10.1007/s10059-013-2190-3.

60. Li M, Yang L, Mu C, Sun Y, Gu Y, Chen D, Liu T, Cao H. Gut microbial metabolome in inflammatory bowel disease: from association to therapeutic perspectives. Comput Struct Biotechnol J. 2022;20:2402–2414. doi:10.1016/j.csbj.2022.03.038.

61. Hosseinkhani F, Heinken A, Thiele I, Lindenburg PW, Harms AC, Hankemeier T. The contribution of gut bacterial metabolites in the human immune signaling pathway of non-communicable diseases. Gut Microbes. 2021;13(1):1–22. doi:10.1080/19490976.2021.1882927.

62. Parada Venegas D, la Fuente Mk D, Landskron G, González MJ, Quera R, Dijkstra G, Harmsen HJM, Faber KN, Hermoso MA. Short chain fatty acids (SCFAs)-mediated gut epithelial and immune regulation and its relevance for inflammatory bowel diseases. Front Immunol. 2019;10:277. doi:10.3389/fimmu.2019.00277.

63. Lamb CA, Kennedy NA, Raine T, Hendy PA, Smith PJ, Limdi JK, Hayee B, Lomer MCE, Parkes GC, Selinger C. et al. British society of gastroenterology consensus guidelines on the management of inflammatory bowel disease in adults. Gut. 2019;68(Suppl 3):s1–s106. doi:10.1136/gutjnl-2019-318484.

64. Scherl EJ, Pruitt R, Gordon GL, Lamet M, Shaw A, Huang S, Mareya S, Forbes WP. Safety and efficacy of a new 3.3 g b.i.d. tablet formulation in patients with mild-to-moderately-active ulcerative colitis: a multicenter, randomized, double-blind, placebo-controlled study. Am J Gastroenterol. 2009;104(6):1452–1459. doi:10.1038/ajg.2009.83.

65. Sandborn WJ, Feagan BG, Hanauer SB. et al. A review of activity indices and efficacy endpoints for clinical trials of medical therapy in adults with Crohn's disease. Gastroenterology. 2002;122(2):512–530. doi:10.1053/gast.2002.31072.

66. Best WR, Becktel JM, Singleton JW, Kern F Jr. Development of a Crohn's disease activity index. National cooperative Crohn's disease study. Gastroenterology. 1976;70(3):439–444. doi:10.1016/S0016-5085(76)80163-1.

67. Joubert R, Mariot V, Dumonceaux J. One-hour universal protocol for mouse genotyping. Muscle & Nerve. 2020;61(6):801–807. doi:10.1002/mus.26841.

68. Hayashi Y, Aoyagi K, Morita I, Yamamoto C, Sakisaka S. Oral administration of mesalazine protects against mucosal injury and permeation in dextran sulfate sodium-induced colitis in rats. Scand J Gastroenterol. 2009;44(11):1323–1331. doi:10.3109/00365520903262414.

69. Varghese F, Bukhari AB, Malhotra R, De A, Aziz SA. IHC profiler: an open source plugin for the quantitative evaluation and automated scoring of immunohistochemistry images of human tissue samples. PLOS ONE. 2014;9(5):e96801. doi:10.1371/journal.pone.0096801.